Mon. Not. R. Astron. Soc. **000**, 1–23 (2008) Printed 15 January 2009 (MN LATEX style file v2.2)

Relativistic Expansion of Magnetic Loops at the Self-similar Stage

Hiroyuki R. Takahashi[1⋆], Eiji Asano[2] and Ryoji Matsumoto[3]
[1] *Graduate School of Science and Technology, Chiba University, 1-33 Yayoi-cho, Inage-ku, Chiba 263-8522, Japan*
[2] *Kwasan and Hida Observatories, Kyoto University, 17 Ohmine-cho, Kita Kazan, Yamashina-ku, Kyoto 607-8471, Japan*
[3] *Department of Physics, Graduate School of Science, Chiba University, 1-33 Yayoi-cho, Inage-ku, Chiba 263-8522, Japan*

Accepted 2007 December 15. Received 2007 December 14; in original form 2007 October 11

ABSTRACT

We obtained self-similar solutions of relativistically expanding magnetic loops taking into account the azimuthal magnetic fields. We neglect stellar rotation and assume axisymmetry and a purely radial flow. As the magnetic loops expand, the initial dipole magnetic field is stretched into the radial direction. When the expansion speed approaches the light speed, the displacement current reduces the toroidal current and modifies the distribution of the plasma lifted up from the central star. Since these self-similar solutions describe the free expansion of the magnetic loops, i.e., $Dv/Dt = 0$, the equations of motion are similar to those of the static relativistic magnetohydrodynamics. This allows us to estimate the total energy stored in the magnetic loops by applying the virial theorem. This energy is comparable to that of the giant flares observed in magnetars.

Key words: relativity - MHD - stars: magnetic field – stars: neutron

1 INTRODUCTION

Soft gamma-ray repeaters (SGRs) are believed to be a young neutron star with strong magnetic fields ($\sim 10^{15}$ G), namely the magnetar (see, e.g., Woods & Thompson 2006; Mereghetti 2008, for review). The magnetic fields inside the magnetar are amplified by the dynamo mechanism at the birth of the neutron star. The Lorentz force stressing the crust of the magnetar balances with the rigidity of the crust. When the critical twist is accumulated, the magnetic twist injected into the magnetar magnetosphere will trigger the expansion of magnetic loops (Thompson & Duncan 2001). The magnetic reconnection taking place inside the expanding magnetic loops can be responsible for SGR flares (Woods et al. 2001; Lyutikov 2006).

Recently, relativistic simulations have been performed to study the dynamics of the magnetospheres of neutron stars (Komissarov 2002; Asano et al. 2005; Spitkovsky 2006; Komissarov 2006). Spitkovsky (2005) reported the results of 2-dimensional relativistic force-free simulations of the magnetar flares triggered by the injection of the magnetic twists at the footpoints of the loops. When the critical twist is accumulated, the magnetic loops expand relativistically. Asano (2007) carried out 2-dimensional relativistic force-free simulations of expanding magnetic loops and showed that the Lorentz factor defined by the drift velocity $\boldsymbol{v}_d = c(\boldsymbol{E} \times \boldsymbol{B})/B^2$ exceeds 10 (see, Uchida 1997, for the definition of the drift velocity). These simulations indicate that the magnetic loops expand self-similarly.

Assuming relativistic force-free dynamics, Lyutikov & Blandford (2003) obtained self-similar solutions of the spherically expanding magnetic shell. Prendergast (2005) found self-similar solutions of the relativistic force-free field. In these studies of force-free dynamics, gas pressure and inertial terms are neglected. In the framework of the relativistic magnetohydrodynamics (MHD), Lyutikov (2002) found self-similar solutions of the spherically expanding magnetic shells. Low (1982) obtained non-relativistic self-similar MHD solutions of the expanding magnetic loops in solar flares or supernovae explosion by assuming axisymmetry. Subsequently, Low (1984) extended his model to the case including toroidal magnetic fields and applied it to solar coronal mass ejections (CMEs). The latter model was employed by Stone et al. (1992) as a test problem to check the validity and accuracy of axisymmetric MHD codes. In magnetar flares, the magnetic loops may be twisted by the shear

⋆ E-mail:takahasi@astro.s.chiba-u.ac.jp

motion at the footpoints of the loops. The shear motion generates Alfvén waves propagating along the field lines. Such twisted magnetic loops expand by the enhanced magnetic pressure by the toroidal magnetic fields. Thus we should include the toroidal magnetic field to study the evolution of magnetic loops during magnetar flares. Also the relativistic effects should be included. The characteristic wave speed in the magnetar magnetosphere approaches the light speed because of the strong magnetic fields. Thus our aim is to obtain relativistic self-similar MHD solutions of expanding magnetic loops taking into account the toroidal magnetic fields by extending the non-relativistic solutions found by Low (1982).

This paper is organized as follows; in § 2, we present the relativistic ideal MHD equations and introduce a self-similar parameter which depends on both radial distance from the centre of the star and time. In § 3, we obtain self-similar solutions. The physical properties of these solutions are discussed in § 4. We summarize the results in § 5.

2 SELF-SIMILAR MHD EQUATIONS

In the following, we take the light speed as unity. The complete set of relativistic ideal MHD equations is

$$\frac{\partial}{\partial t}(\gamma\rho) + \nabla\cdot(\gamma\rho\boldsymbol{v}) = 0, \tag{1}$$

$$\rho\gamma\left[\frac{\partial}{\partial t} + (\boldsymbol{v}\cdot\nabla)\right](\xi\gamma\boldsymbol{v}) = -\nabla p + \rho_e\boldsymbol{E} + \boldsymbol{j}\times\boldsymbol{B} - \frac{GM\rho\gamma}{r^2}\boldsymbol{e}_r, \tag{2}$$

$$\left[\frac{\partial}{\partial t} + (\boldsymbol{v}\cdot\nabla)\right]\left(\ln\frac{p}{\rho^\Gamma}\right) = 0, \tag{3}$$

$$\nabla\cdot\boldsymbol{E} = 4\pi\rho_e, \tag{4}$$

$$\nabla\cdot\boldsymbol{B} = 0, \tag{5}$$

$$\frac{\partial\boldsymbol{B}}{\partial t} + \nabla\times\boldsymbol{E} = 0, \tag{6}$$

$$\frac{\partial\boldsymbol{E}}{\partial t} = \nabla\times\boldsymbol{B} - 4\pi\boldsymbol{j}, \tag{7}$$

$$\boldsymbol{E} = -\boldsymbol{v}\times\boldsymbol{B}, \tag{8}$$

where $\boldsymbol{E}, \boldsymbol{B}, \boldsymbol{j}, \boldsymbol{v}, \gamma, \rho_e, \rho, p, \Gamma$ are the electric field, the magnetic field, the current density, the velocity, the Lorentz factor, the charge density, the mass density, the pressure and the specific heat ratio, respectively. The vector $\boldsymbol{e}_r$ is a unit vector in the radial direction. We include the gravity by a point mass M as an external force. Here G is the gravitational constant, and r is the distance from the centre of the star. The relativistic specific enthalpy ξ is defined as

$$\xi = \frac{\epsilon + p}{\rho} = 1 + \frac{\Gamma}{\Gamma - 1}\frac{p}{\rho}, \tag{9}$$

where ϵ is the energy density of matter including the photon energy coupled with the plasma. In SGR outbursts, since the luminosity much exceeds the Eddington luminosity, radiation energy density can exceed the thermal energy of the plasma. In the following pressure p includes the contribution from the radiation pressure.

In this paper, we consider relativistic self-similar expansions of magnetic loops which started expansion at $t = t_\mathrm{s}$ by loss of dynamical equilibrium and entered into a self-similar stage at $t = t_0 > t_\mathrm{s}$. We do not consider the evolution of the loops before $t = t_0$.

For simplicity, we ignore the stellar rotation and assume axisymmetry. We can express the axisymmetric magnetic field in terms of two scalar functions $\tilde{A}$ and B as

$$\boldsymbol{B} = \frac{1}{r\sin\theta}\left(\frac{1}{r}\frac{\partial\tilde{A}}{\partial\theta}, -\frac{\partial\tilde{A}}{\partial r}, B\right), \tag{10}$$

in the polar coordinates (r, θ, ϕ). The scalar function $\tilde{A}(t, r, \theta)$ denotes the magnetic flux, whose contours coincide with magnetic field lines projected on to the $r-\theta$ plane.

We further assume that the fluid flow is purely radial;

$$\boldsymbol{v} = v(t, r, \theta)\,\boldsymbol{e}_r. \tag{11}$$

Equations (1), (2), (3), and (6) are then expressed as

$$\frac{\partial(\rho\gamma)}{\partial t} + \frac{1}{r^2}\frac{\partial(r^2\rho\gamma v)}{\partial r} = 0, \tag{12}$$

$$\rho\gamma\left[\frac{\partial}{\partial t} + v\frac{\partial}{\partial r}\right](\xi\gamma v) = -\frac{\partial p}{\partial r} - \frac{1}{4\pi r^2\sin^2\theta}\left\{\frac{\partial\tilde{A}}{\partial r}\left[\left(\hat{\mathcal{L}}_{(r,\theta)}\tilde{A}\right) + \frac{\partial}{\partial t}\left(v\frac{\partial\tilde{A}}{\partial r}\right)\right] + B\left[\frac{\partial B}{\partial r} + \frac{\partial(vB)}{\partial t}\right]\right\} - \frac{GM\rho\gamma}{r^2}, \tag{13}$$

$$4\pi r^2 \sin^2\theta \frac{\partial p}{\partial \theta} + (1-v^2)B\frac{\partial B}{\partial \theta} + \frac{\partial \tilde{A}}{\partial \theta}\left[\left(\hat{\mathcal{L}}_{(r,\theta)}\tilde{A}\right) + \frac{\partial}{\partial t}\left(v\frac{\partial \tilde{A}}{\partial r}\right)\right] - vB^2\frac{\partial v}{\partial \theta} = 0, \tag{14}$$

$$(1-v^2)\frac{\partial \tilde{A}}{\partial r}\frac{\partial B}{\partial \theta} - \frac{\partial \tilde{A}}{\partial \theta}\left[\frac{\partial B}{\partial r} + \frac{\partial (vB)}{\partial t}\right] - vB\frac{\partial \tilde{A}}{\partial r}\frac{\partial v}{\partial \theta} = 0, \tag{15}$$

$$\left[\frac{\partial}{\partial t} + v\frac{\partial}{\partial r}\right]\left(\ln\frac{p}{\rho^{\Gamma}}\right) = 0, \tag{16}$$

$$\frac{\partial \tilde{A}}{\partial t} + v\frac{\partial \tilde{A}}{\partial r} = 0, \tag{17}$$

$$\frac{\partial B}{\partial t} + \frac{\partial (vB)}{\partial r} = 0, \tag{18}$$

where we used the MHD condition given by (8) and introduced the operator

$$\hat{\mathcal{L}}_{(r,\theta)} \equiv \frac{\partial^2}{\partial r^2} + \frac{\sin\theta}{r^2}\frac{\partial}{\partial \theta}\left(\frac{1}{\sin\theta}\frac{\partial}{\partial \theta}\right). \tag{19}$$

Since our aim is to obtain self-similar solutions of these relativistic MHD equations, we assume that the time evolution is governed by the self-similar variable:

$$\eta = \frac{r}{Z(t)}, \tag{20}$$

where $Z(t)$ is an arbitrary function of time. We further assume that the flux function $\tilde{A}$ depends on time t and the radial distance r through the self-similar variable η, as

$$\tilde{A}(t,r,\theta) = \tilde{A}(\eta,\theta). \tag{21}$$

When equation (21) is satisfied, the radial velocity v has a form

$$v = \eta\dot{Z}, \tag{22}$$

from equation (17). Here dot denotes the time derivative. Equation (22) implies that the radial velocity v does not depend on the polar angle θ. It then follows from equations (12) and (18) that

$$\rho(t,r,\theta)\gamma(t,r) = Z^{-3}(t)D(\eta,\theta), \tag{23}$$

$$B(t,r,\theta) = Z^{-1}(t)Q(\eta,\theta), \tag{24}$$

where Q and D are arbitrary functions of η and θ. These relations indicate that the magnetic flux and the total mass are conserved. Next we take the pressure p as $p(t,r,\theta) = Z^l P(\eta,\theta)$. Substituting this equation into equations (14) and (16), we obtain

$$4\pi\eta^2 Z^{l+4}\sin^2\theta\frac{\partial P}{\partial \theta} + \frac{\partial \tilde{A}}{\partial \theta}\left[\hat{\mathcal{L}}_{(\eta,\theta)}\tilde{A} + \left(\eta Z\ddot{Z} - 2\eta\dot{Z}^2\right)\frac{\partial \tilde{A}}{\partial \eta} - \eta^2\dot{Z}^2\frac{\partial^2\tilde{A}}{\partial \eta^2}\right] + (1-\eta^2\dot{Z}^2)Q\frac{\partial Q}{\partial \theta} = 0, \tag{25}$$

$$\frac{\Gamma\eta^2 Z\ddot{Z}}{1-\eta^2\dot{Z}^2} + (3\Gamma + l) = 0, \tag{26}$$

where we introduced an operator $\hat{\mathcal{L}}_{(\eta,\theta)}$:

$$\hat{\mathcal{L}}_{(\eta,\theta)} \equiv \frac{\partial^2}{\partial \eta^2} + \frac{\sin\theta}{\eta^2}\frac{\partial}{\partial \theta}\left(\frac{1}{\sin\theta}\frac{\partial}{\partial \theta}\right) = \frac{1}{Z^2}\hat{\mathcal{L}}_{(r,\theta)}. \tag{27}$$

To satisfy these equations, p, Z and Γ should have forms

$$p(t,r,\theta) = Z^{-4}P(\eta,\theta), \tag{28}$$

$$Z(t) = t, \tag{29}$$

and

$$\Gamma = \frac{4}{3}. \tag{30}$$

This adiabatic index corresponds to the radiation pressure dominant plasma. Thus our model can describe the evolution of a fireball confined by magnetic fields.

Equations (23) and (28) indicate that the magnetic loops expand adiabatically. By using equations (22), (23), (24), (28), (29) and (30), equations (13), (15) and (25) are expressed as

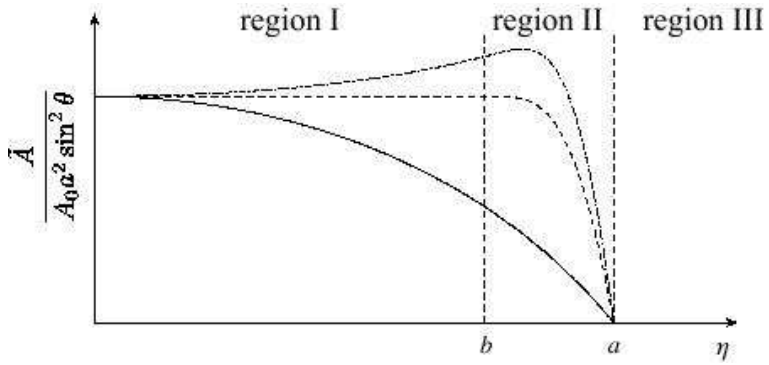

Figure 1. The flux function $\tilde{A}$ as a function of η for the dipolar solution (solid curve), the shell solution (dashed curve), and the flux rope solution (dot-dashed curve). The parameters a and b denote the outer and inner boundaries of the shell, respectively.

$$D(\eta,\theta) = \frac{\eta^2}{GM}\left\{\frac{4\eta P}{1-\eta^2} - \frac{\partial P}{\partial \eta} - \frac{1}{4\pi\eta^2\sin^2\theta}\left[\frac{\partial \tilde{A}}{\partial \eta}\left(\hat{\mathcal{L}}_{(\eta,\theta)}\tilde{A} - \frac{\partial}{\partial \eta}\left(\eta^2\frac{\partial \tilde{A}}{\partial \eta}\right)\right) + Q\frac{\partial}{\partial \eta}\left(Q(1-\eta^2)\right)\right]\right\}, \tag{31}$$

$$(1-\eta^2)\frac{\partial \tilde{A}}{\partial \eta}\frac{\partial Q}{\partial \theta} - \frac{\partial \tilde{A}}{\partial \theta}\frac{\partial}{\partial \eta}\left[(1-\eta^2)Q\right] = 0, \tag{32}$$

$$4\pi\eta^2\sin^2\theta\frac{\partial P}{\partial \theta} + \frac{\partial \tilde{A}}{\partial \theta}\left[\hat{\mathcal{L}}_{(\eta,\theta)}\tilde{A} - \frac{\partial}{\partial \eta}\left(\eta^2\frac{\partial \tilde{A}}{\partial \eta}\right)\right] + (1-\eta^2)Q\frac{\partial Q}{\partial \theta} = 0. \tag{33}$$

From equation (32), a formal solution of Q is obtained as

$$Q(\eta,\theta) = \frac{\mathcal{G}(\tilde{A})}{1-\eta^2}, \tag{34}$$

where $\mathcal{G}$ is an arbitrary function.

Self-similar solutions can be constructed as follows. First we prescribe an arbitrary function $\tilde{A}(\eta,\theta)$ (or $Q(\eta,\theta)$). Then, equation (32) determines the function $Q(\eta,\theta)$ (or $\tilde{A}(\eta,\theta)$). Functions $\tilde{A}$ and Q determine the pressure $P(\eta,\theta)$ according to equation (33). Finally, the density function $D(\eta,\theta)$ is obtained by equation (31).

Note that from the equation (22) and (29), the radial velocity has a simple form as

$$v = \frac{r}{t}. \tag{35}$$

Since the time derivative of the velocity becomes zero, i.e., $D\boldsymbol{v}/Dt = 0$, equations (31)-(33) describe the freely expanding solution. This means that there is a reference frame that all forces balance. By substituting equations (23), (24), (28), (29), and (35) into the equations of motion (2), we obtain

$$\frac{\Gamma}{\Gamma-1}\frac{\gamma^2 v^2 p}{r}\boldsymbol{e}_r - \nabla p + \rho_e\boldsymbol{E} + \boldsymbol{j}\times\boldsymbol{B} - \frac{GM\rho\gamma}{r^2}\boldsymbol{e}_r = 0. \tag{36}$$

The first term on the left hand side comes from the inertia. For convenience, we call this term as a thermal inertial term throughout this paper. When we neglect the terms of order $(v/c)^2$, equation (36) reduces to the equations of the force balance in non-relativistic MHD.

3 SELF-SIMILAR SOLUTIONS

In the previous section, we derived relativistic self-similar MHD equations, (31), (32) and (33). In this section, we obtain solutions of these equations by imposing appropriate boundary conditions. As mentioned in the previous section, the toroidal magnetic field, the pressure, and the gas density are calculated by assigning the flux function $\tilde{A}(\eta,\theta)$. In the following, we introduce three kinds of flux functions and obtain explicit forms of other variables.

3.1 Construction of Solutions

We assume that the expanding magnetic loops have a spherical outer boundary at $r = R(t)$.

A simple solution of the expanding magnetic loops is that the poloidal magnetic field is dipolar near the surface of the star (Low 1982). The magnetic field should be tangential to the spherical surface $r = R(t)$ at all time. Such a solution can be constructed by

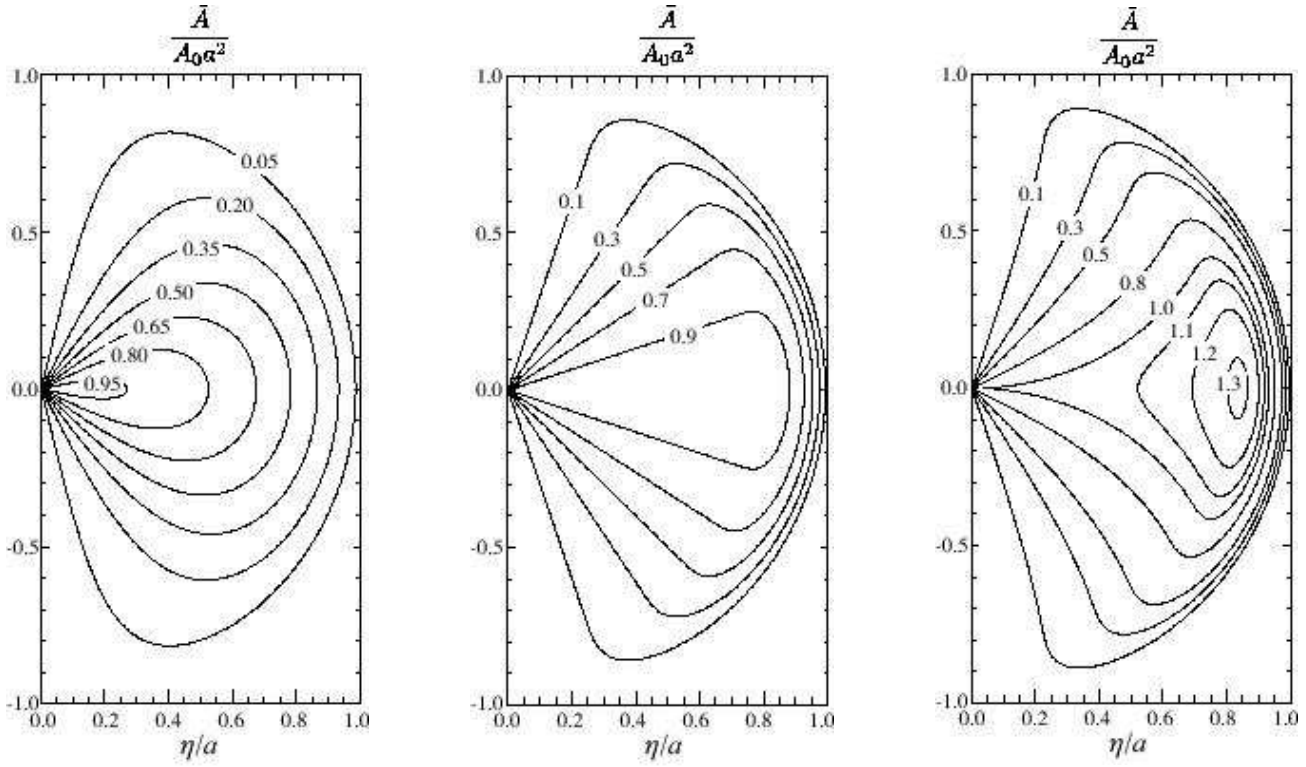

Figure 2. Contour plots of the magnetic flux $\tilde{A}$ which constructs the dipolar, shell, and flux rope solutions from left to right, respectively. The parameters are taken as $a = 0.8$, $b/a = 0.7$, and $k = \pi/[4(a-b)]$.

$$\tilde{A}(\eta,\theta) = A_0 \frac{a^2-\eta^2}{\sqrt{1-\eta^2}} \sin^2\theta, \tag{37}$$

where A_0 and a are constants. The radius $R(t)$ where $\tilde{A} = 0$ is given by

$$R(t) = at. \tag{38}$$

We hereafter call the solution constructed from equation (37) as *dipolar solution*.

Solid curve in Fig. 1 shows the flux function $\tilde{A}$ as a function of η for the dipolar solution. Contour plots of $\tilde{A}$ for dipolar solution is shown in the left panel of Fig. 2.

When the flux function is given by equation (37), the magnetic flux crossing the annulus at the equatorial plane $\theta = \pi/2$ decreases with radius (see Fig. 1). In actual MHD explosion, the magnetic flux can be swept up into a thin shell just behind the loop top. The shell boundaries are assumed to be at $r = bt$ and $r = at$ (region II, see Fig. 1). Such a self-similar field can be constructed by

$$\tilde{A}(\eta,\theta) = \begin{cases} A_0 a^2 \sin^2\theta, & (\text{region I} : \eta \leqq b), \\ A_0 a^2 \Lambda(\eta) \sin^2\theta, & (\text{region II} : b < \eta \leqq a), \end{cases} \tag{39}$$

where

$$\Lambda(\eta) = 1 - \frac{\sin^4 T(\eta)}{\sin^4 T(a)}, \tag{40}$$

$$T(\eta) = k(\eta - b), \tag{41}$$

and a, b and k are constants (Low 1982). The flux functions in region I ($\eta \leqq b$) and region II ($b < \eta \leqq a$) are connected smoothly at $\eta = b$. The loop boundary locates at $r = at$, where $\tilde{A} = 0$.

The flux function for this solution is shown by a dashed curve in Fig. 1. It can be easily shown that the magnetic field lines projected on to the $r-\theta$ plane are all radial in region I. We call the solution constructed from equation (39) as *shell solution*. The middle panel of Fig. 2 shows the contours of $\tilde{A}$ for the shell solution.

Another solution is that we call *flux rope solution*. As the magnetic loops expand, a current sheet is formed inside the magnetic loops. It is suggested that the magnetic reconnection taking place in the current sheet is responsible for the SGR flares (Woods et al. 2001; Lyutikov 2006). When the magnetic reconnection takes place, flux ropes (namely plasmoids) are formed inside magnetic loops. The flux function should then have a local maximum inside the flux rope. Such a solution can

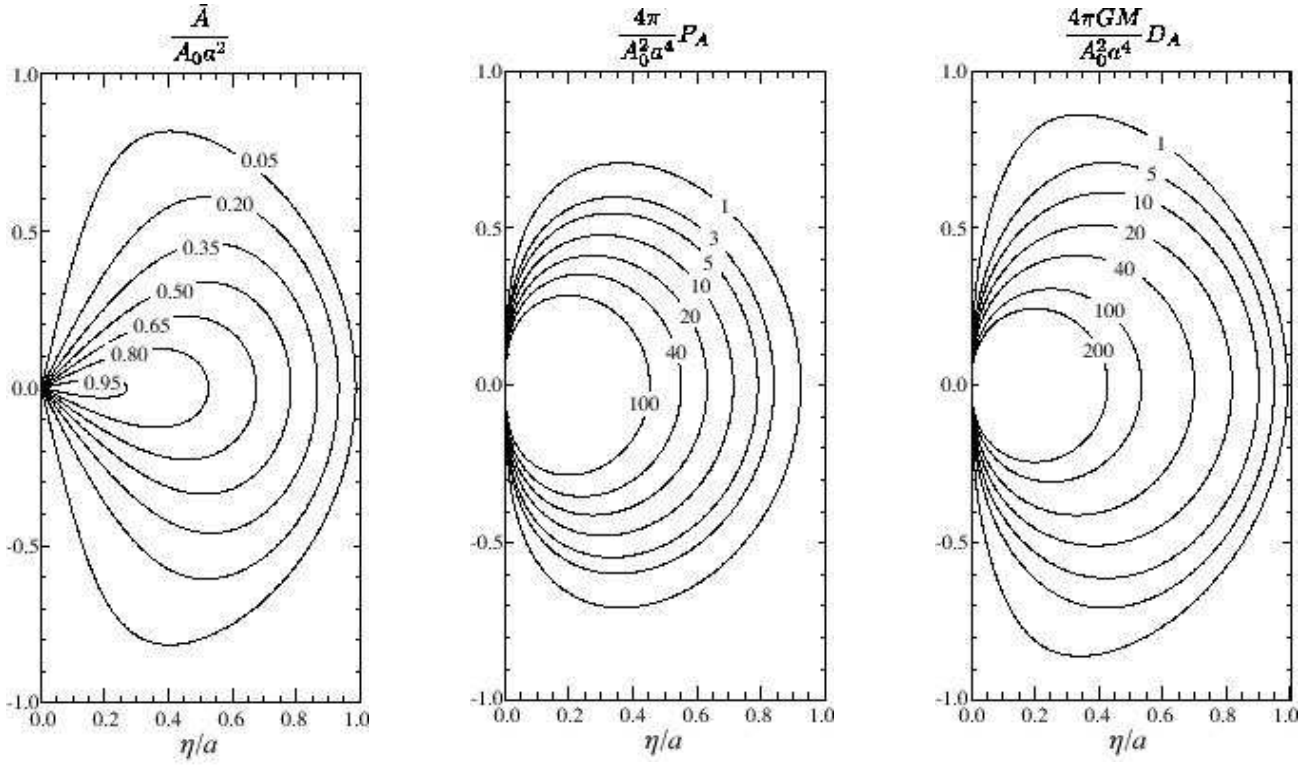

Figure 3. Contour plots of the magnetic flux $\tilde{A}$ (left), the poloidal part of the pressure P_A (centre), and that of the gas density D_A(right) for the dipolar solution in $\eta/a - \theta$ plane when $a = 0.8$.

be constructed by

$$\tilde{A}(\eta,\theta) = \begin{cases} \dfrac{A_0 a^2}{\sqrt{1-\eta^2}} \sin^2\theta, & (\text{region I} : \eta \leqq b), \\ \dfrac{A_0 a^2}{\sqrt{1-\eta^2}} \Lambda(\eta) \sin^2\theta, & (\text{region II} : b < \eta \leqq a), \end{cases} \tag{42}$$

where A_0, a are constants and $\Lambda(\eta)$ is given by equation (40). This function is shown by a dot-dashed curve in Fig. 1. It has a local maximum in the domain $b < \eta < a$ (see Fig. 1). The contours of $\tilde{A}$ for the flux rope solution is shown in the right panel of Fig. 2. Flux ropes appear behind the shell.

3.2 Dipolar Solutions

Dipolar solutions are constructed by the flux function specified by equation (37). The azimuthal magnetic fields can be obtained by substituting equation (37) into equation (32) as

$$Q(\eta,\theta) = \sum_n Q_{0,n} \frac{(a^2-\eta^2)^{\frac{n}{2}}}{(1-\eta^2)^{1+\frac{n}{4}}} \sin^n\theta, \tag{43}$$

where $Q_{0,n}$ are constants. Note that the solutions (37) and (43) satisfy the formal solution given by equation (34). Substituting equations (37) and (43) into equation (33), we obtain the pressure function P:

$$P(\eta,\theta) = P_0(\eta) + P_A(\eta,\theta) + P_Q(\eta,\theta), \tag{44}$$

where $P_0(\eta)$ is an arbitrary function arisen from the integration and P_A and P_Q are given by

$$P_A(\eta,\theta) = \frac{A_0^2}{4\pi\eta^4} \frac{a^2-\eta^2}{(1-\eta^2)^2} (2a^2 - 3a^2\eta^2 - \eta^4 + 2\eta^6) \sin^2\theta, \tag{45}$$

$$P_Q(\eta,\theta) = \begin{cases} -\displaystyle\sum_{m+n\neq 2} \frac{n Q_{0,m} Q_{0,n}}{4\pi(m+n-2)} \frac{(a^2-\eta^2)^{\frac{m+n}{2}}}{\eta^2(1-\eta^2)^{1+\frac{m+n}{4}}} \sin^{m+n-2}\theta, & \text{for } m+n \neq 2, \\ -\displaystyle\sum_{m+n=2} \frac{n Q_{0,m} Q_{0,n}}{4\pi} \frac{a^2-\eta^2}{\eta^2(1-\eta^2)^{\frac{3}{2}}} \log(\sin\theta), & \text{for } m+n = 2. \end{cases} \tag{46}$$

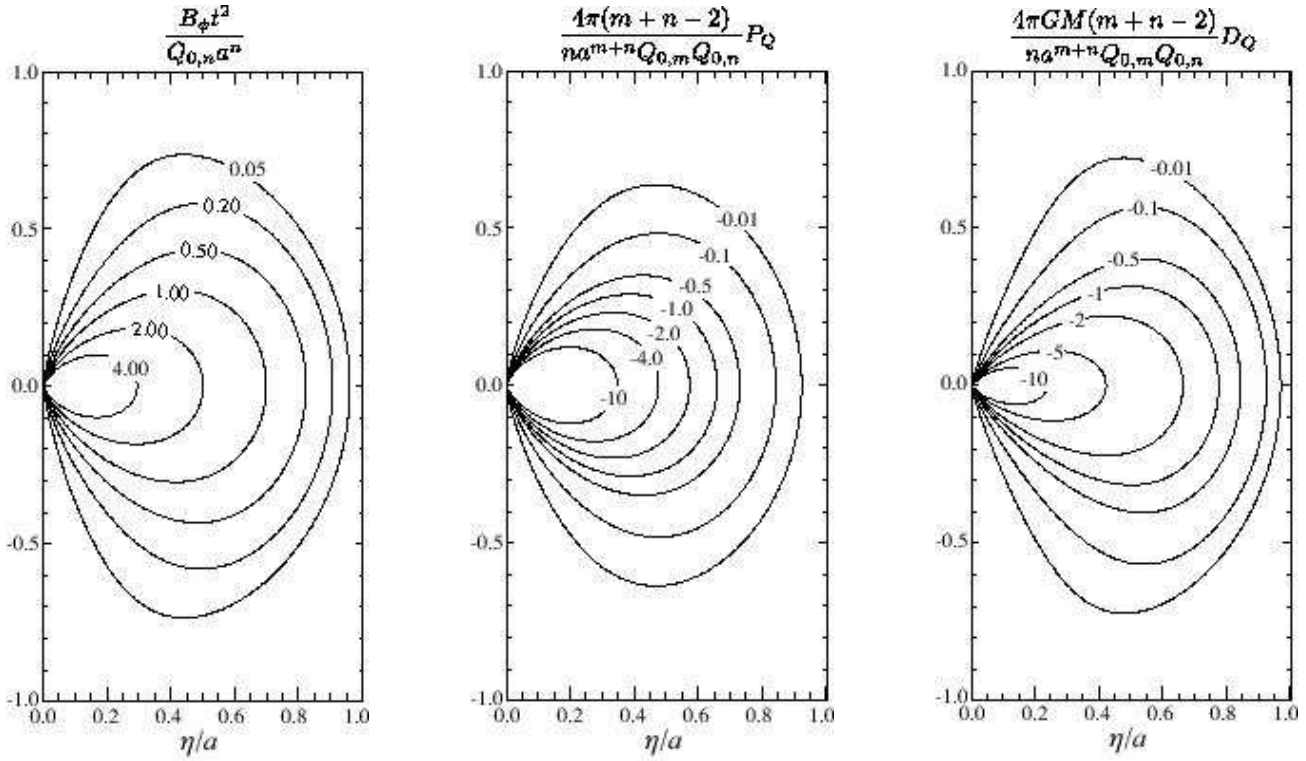

Figure 4. Contour plots of the toroidal magnetic field (left), the toroidal part of the pressure P_Q (centre), and that of the density D_Q(right) for the dipolar solution in $\eta/a-\theta$ plane when $a=0.8$ and $m=n=4$.

Substituting equations (37), (43), (44), (45), and (46) into (31), the density function D can be determined as

$$D(\eta,\theta)=D_0(\eta)+D_A(\eta,\theta)+D_Q(\eta,\theta), \tag{47}$$

where

$$D_0(\eta)=\frac{\eta^2}{GM}\left(\frac{4\eta P_0}{1-\eta^2}-\frac{dP_0}{d\eta}\right), \tag{48}$$

$$D_A(\eta,\theta)=\frac{A_0^2}{4\pi GM\eta^3}\frac{(a^2-\eta^2)}{(1-\eta^2)^3}\left[a^2(8-12\eta^2+3\eta^4)-\eta^6(5-6\eta^2)\right]\sin^2\theta, \tag{49}$$

$$D_Q(\eta,\theta)=\begin{cases}-\displaystyle\sum_{m+n\neq 2}\frac{nQ_{0,m}Q_{0,n}}{4\pi GM(m+n-2)}\frac{(a^2-\eta^2)^{\frac{m+n-2}{2}}(2a^2-a^2\eta^2-\eta^4)}{\eta(1-\eta^2)^{2+\frac{m+n}{4}}}\sin^{(m+n-2)}\theta, & \text{for } m+n\neq 2,\\ -\displaystyle\sum_{m+n=2}\frac{nQ_{0,m}Q_{0,n}}{8\pi GM}\frac{-\eta^2(2-a^2-\eta^2)+2(2a^2-a^2\eta^2-\eta^4)\log(\sin\theta)}{\eta(1-\eta^2)^{\frac{5}{2}}}, & \text{for } m+n=2.\end{cases} \tag{50}$$

The parameters m and n correspond to the Fourier modes in the θ direction. These parameters should be determined by the boundary condition on the surface of the central star where magnetic twist is injected.

Equation (44) and (47) indicate that the solution consists of three parts, P_0, P_A and P_Q (or D_0, D_A and D_Q). The arbitrary function $P_0(\eta)$ describes an isotropic pressure in the region $r<R(t)$. The isotropic density profile $D_0(\eta)$ is related to P_0 through equation (48). This equation is similar to that in non-relativistic model (Low 1982). In the non-relativistic model, gravity is supported by the gradient of $P_0(\eta)$. In the relativistic case, relativistic correction of the plasma inertia cannot be ignored. This effect is included in the first term in the right hand side of equation (48). Other functions P_A and P_Q (or D_A and D_Q) come from the interaction with the electromagnetic force. Note that the plasma pressure P_Q, which balances with the electromagnetic force produced by the toroidal magnetic field, is always negative. This suggests that the pressure is smaller for larger toroidal magnetic fields.

Fig. 3 shows the contour plots of the magnetic flux $\tilde{A}$ (left), the poloidal part of the pressure P_A (centre), and that of the gas density D_A (right), while Fig. 4 shows the contour plots of the toroidal magnetic field B_ϕ (left), the toroidal part of the pressure P_Q (centre), and that of the gas density D_Q (right) in the $\eta/a-\theta$ plane for $m=n=4$ and $a=0.8$.

The magnetic field is explicitly expressed as

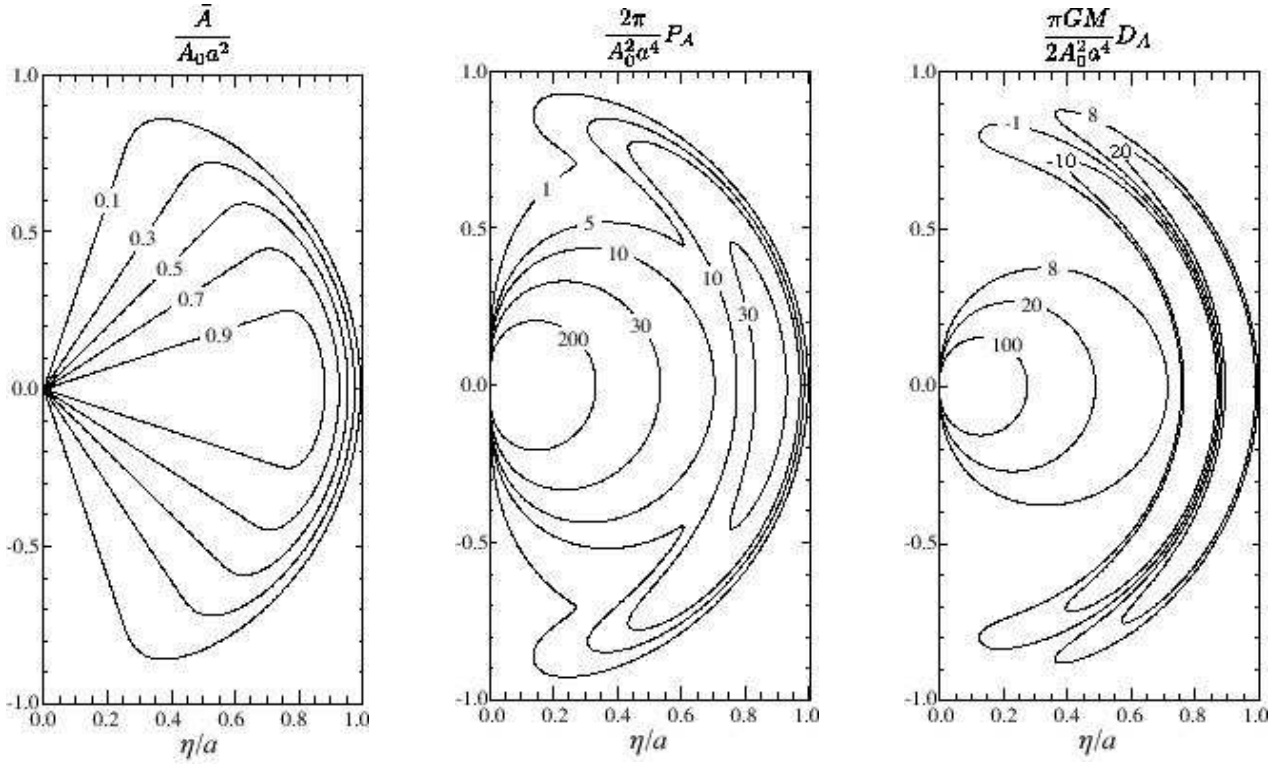

Figure 5. Contour plots of the magnetic flux $\tilde{A}$ (left), the poloidal part of the pressure P_A (centre), and that of the gas density D_A (right) for the shell solution in $\eta/a - \theta$ plane when $a = 0.8$ and $b = 0.75a$.

$$\boldsymbol{B} = \frac{2A_0}{r^2}\frac{a^2-(r/t)^2}{\sqrt{1-(r/t)^2}}\cos\theta\boldsymbol{e}_r + \frac{A_0}{t^2}\frac{2-a^2-(r/t)^2}{[1-(r/t)^2]^{\frac{3}{2}}}\sin\theta\boldsymbol{e}_\theta + \sum_n \frac{Q_{0,n}}{rt}\frac{\left[a^2-(r/t)^2\right]^{\frac{n}{2}}}{[1-(r/t)^2]^{1+\frac{n}{4}}}\sin^{n-1}\theta\boldsymbol{e}_\phi, \tag{51}$$

where $\boldsymbol{e}_r$, $\boldsymbol{e}_\theta$, and $\boldsymbol{e}_\phi$ are unit vectors in r, θ, and ϕ directions in the polar coordinate, respectively. Note that B_r and B_ϕ are zero at $r = R(t)$ but B_θ is not zero and it depends on time when $a \neq 1$. We will discuss the physical meaning of this result later in §3.3.

In later stage, the magnetic field becomes stationary,

$$\lim_{t\to\infty}\boldsymbol{B} = \frac{2A_0a^2}{r^2}\cos\theta\boldsymbol{e}_r, \tag{52}$$

and the magnetic field becomes radial. In the limit $t \gg r$, the pressure and the gas density inside the magnetic loop are given by

$$\lim_{t\to\infty} p = \frac{A_0^2a^4}{2\pi r^4}\sin^2\theta + \frac{1}{r^4}\left(P_0\eta^4\right)\Big|_{\eta=0}, \tag{53}$$

$$\lim_{t\to\infty} \rho = \frac{2A_0^2a^4}{\pi GMr^3}\sin^2\theta + \frac{1}{r^3}\left(D_0\eta^3\right)\Big|_{\eta=0}. \tag{54}$$

Since the toroidal magnetic field tends to be zero in this limit, the pressure and density do not depend on the amplitude of the toroidal magnetic fields.

3.3 Shell Solutions

Shell solutions are constructed from the flux function (39). By substituting equation (39) into equation (32), the function Q can be obtained as

$$Q^I(\eta,\theta) = Q_0^I\frac{f(\theta)}{1-\eta^2}, \tag{55}$$

$$Q^{II}(\eta,\theta) = \sum_n \frac{Q_{0,n}^{II}}{1-\eta^2}\left[\sin^4 T(a) - \sin^4 T(\eta)\right]^{\frac{n}{2}}\sin^n\theta, \tag{56}$$

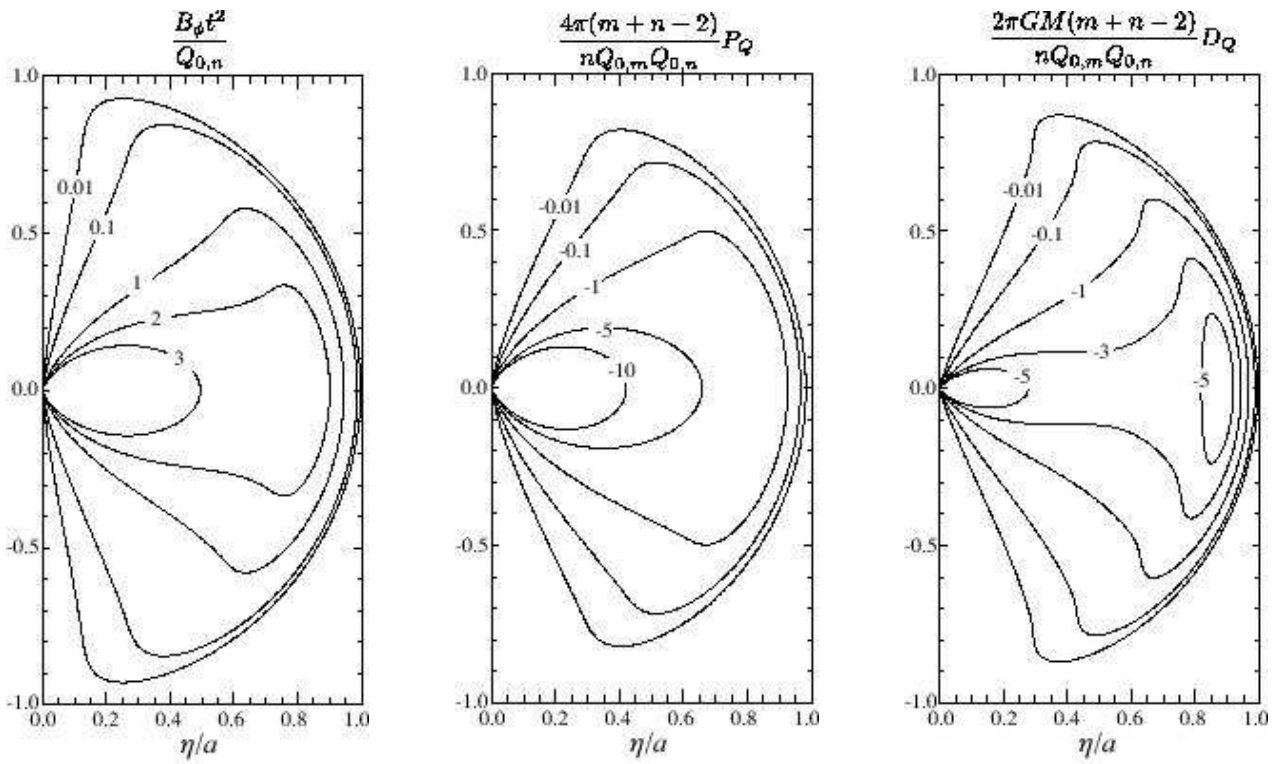

Figure 6. Contour plots of the toroidal magnetic field B_ϕ (left), the toroidal part of the pressure P_Q (centre), and that of the gas density D_Q (right) for the shell solution in $\eta/a - \theta$ plane when $a = 0.8, b = 0.75a$, and $n = m = 4$.

where $f(\theta)$ is an arbitrary function of θ, and Q_0^I and $Q_{0,n}^{II}$ are constants. The subscripts I and II mean that the function is defined in region I and in region II, respectively. The arbitrary function $f(\theta)$ can be determined by applying the boundary condition that magnetic field should be connected smoothly at $\eta = b$,

$$Q^I(\eta = b, \theta) = Q^{II}(\eta = b, \theta). \tag{57}$$

By using the boundary condition, the function f is given by

$$f(\theta) = \sum_n \sin^n \theta. \tag{58}$$

and the function Q^I is obtained as

$$Q^I(\eta, \theta) = \sum_n Q_{0,n}^I \frac{\sin^n \theta}{1 - \eta^2}. \tag{59}$$

The constants $Q_{0,n}^I$ and $Q_{0,n}^{II}$ should be related by

$$Q_{0,n} \equiv Q_{0,n}^I = Q_{0,n}^{II} \sin^{2n} T(a). \tag{60}$$

from the boundary condition (57). Substituting equations (39), (56), (59) and (60) into equation (33), we obtain the pressure function $P(\eta, \theta)$. The density function $D(\eta, \theta)$ is obtained from equation (31). The functions Q, P, and D obtained in region I and region II are given in appendix A.

The pressure and the gas density consist of three parts, the isotropic part P_0 and parts representing the interaction with the electromagnetic force by the poloidal and toroidal components of the magnetic field, P_A and P_Q, similarly to the dipolar solutions (see equations (A2) and (A9), for the pressure and equations (A5) and (A12) for the gas density).

Fig. 5 shows the contour plots of the magnetic flux $\tilde{A}$ (left), the poloidal part of the pressure P_A (centre), and that of the gas density D_A (right) in $\eta/a - \theta$ plane. Fig. 6 shows contour plots of the toroidal magnetic field B_ϕ (left), the toroidal part of the pressure P_Q (centre), and that of the gas density D_Q (right) in $\eta/a - \theta$ plane. The parameters are taken to be $a = 0.8$, $b = 0.75a$, and $m = n = 4$ in both figures. A shell structure appears behind the loop top.

The pressure P_Q is always negative (see equations (A4) and (A11) and the middle panel of Fig. 6) and its amplitudes is proportional to that of the toroidal magnetic fields, $Q_{0,n}$. This indicates that the pressure is smaller for a larger toroidal magnetic field.

The magnetic field is explicitly given by

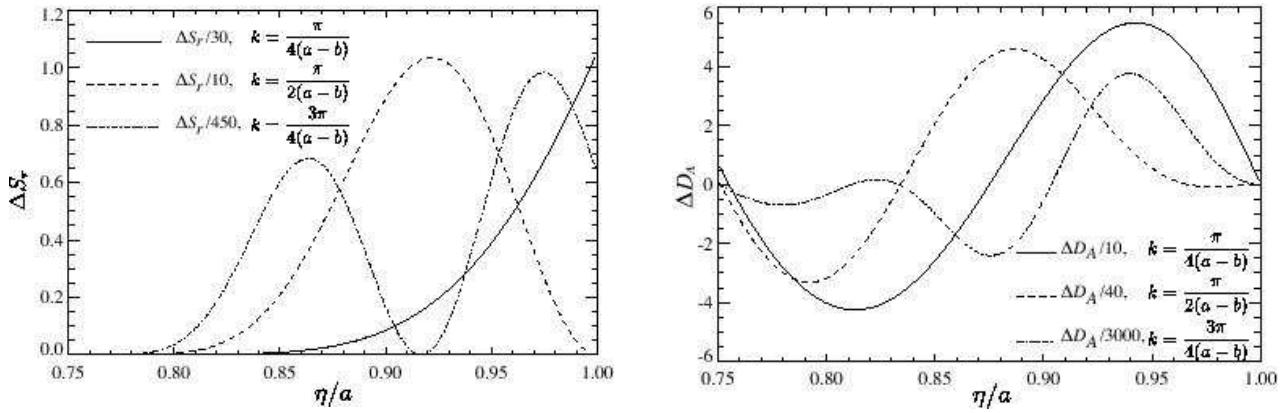

Figure 7. Distributions of the Poynting flux $\Delta S_r \equiv \pi r^4 S_r/(A_0^2 a^4 \sin^2\theta)$ (left) and $\Delta D_A \equiv D_A \pi GM\eta^3(1-\eta^2)/[2A_0^2 a^4 \sin^2\theta]$ (right) for the shell solutions, where $\boldsymbol{S}_r$ is the Poynting flux in the radial direction. Solid curves show for $k = \pi/[4(a-b)]$, while dashed and dot-dashed ones for $k = \pi/[2(a-b)]$, and $k = 3\pi/[4(a-b)]$, respectively. Here we take $Q_{0,n} = 0$.

$$\boldsymbol{B} = \begin{cases} \dfrac{2A_0 a^2}{r^2}\cos\theta \boldsymbol{e}_r + \displaystyle\sum_n Q_{0,n}\frac{t}{r(t^2-r^2)}\sin^{n-1}\theta \boldsymbol{e}_\phi, & (\eta \leqq b), \\ \dfrac{2A_0 a^2}{r^2}\Lambda\,(r/t)\cos\theta \boldsymbol{e}_r + \dfrac{4A_0 a^2}{rt}k\dfrac{\sin^3 T(r/t)\cos T(r/t)}{\sin^4 T(a)}\sin\theta \boldsymbol{e}_\theta + \displaystyle\sum_n Q_{0,n}\Lambda^{\frac{n}{2}}\,(r/t)\,\frac{t\sin^{n-1}\theta}{r(t^2-r^2)}\boldsymbol{e}_\phi, & (b < \eta \leqq a). \end{cases} \tag{61}$$

Similarly to the dipolar solution, the shell solutions have the parameter m which corresponds to the Fourier modes in the polar angle θ. These modes and the corresponding amplitude $Q_{0,m}$ of the toroidal magnetic fields should be determined by the boundary condition at the surface of the central star where the magnetic twist is injected.

In contrast to the dipolar solution, the magnetic field lines do not cross the equatorial plane in region I (see the left panel in Fig. 5). Note that in the limit that $t \gg r$, the magnetic fields and plasma distribution approach those of the dipolar solution, given by (52), (53) and (54).

At the boundary $r = R(t)$, the field components B_r and B_ϕ are exactly zero, but B_θ is not zero. Since the Poynting flux $\boldsymbol{S} = (\boldsymbol{E}\times\boldsymbol{B})/(4\pi)$ is not zero at $r = R(t)$, the energy flux will be transmitted to the region outside the boundary at $r = R(t)$. When $\cos T(a) = 0$, since the magnetic field vanishes at $r = R(t)$, the energy is not transferred to $r > R(t)$. This happens when the constant k is given by

$$k = \frac{(2l+1)}{2}\frac{\pi}{a-b}, \tag{62}$$

where l is an integer number.

Fig. 7 shows the distributions of the Poynting flux $\Delta S_r = r^4\pi S_r/(A_0^2 a^4\sin^2\theta)$ (left panel) and $\Delta D_A \equiv D_A\pi GM\eta^3(1-\eta^2)/[2A_0^2 a^4\sin^2\theta]$ (right panel) for $a = 0.8$, $b/a = 0.75$, and $B_\phi = 0$ for shell solutions. Solid curve denotes that for $k = \pi/[4(a-b)]$, while dashed and dot-dashed ones do for $k = \pi/[2(a-b)]$ and $k = 3\pi/[4(a-b)]$, respectively. When k satisfies equation (62), $B_\theta(t, r = at, \theta) = 0$ and thus $S_r(t, r = at, \theta) = 0$. Electromagnetic energy is not transmitted ahead of the loop top. When k does not satisfy equation (62), the Poynting flux S_r at $r = at$ is not zero and the electromagnetic energy is transmitted to $r > at$. The physical interpretation of the condition given in equation (62) is as follows.

Let us consider the MHD waves propagating inside the magnetic loops. The MHD waves consist of the forward wave $B_{\rm for}$ and the reflected wave $B_{\rm ref}$ ($B_{\rm for}$ and $B_{\rm ref}$ are the magnetic fields in the poloidal plane). When the wave $B_{\rm leak}^{III}$ is transmitted to region III (see Fig. 8), the electromagnetic energy can be converted to the kinetic and thermal energies in region III. The magnetic field B_θ given in equation (61) can be expressed by the superposition of the forward and reflected waves. When the density enhancement appears ahead of the magnetic loop in region II, the forward waves can be partially reflected by it. The condition for the perfect reflection should be determined by the wavelength λ and the thickness of the density enhancement $d \sim (a-b)t$. This situation is analogous to the enhancement of the reflection rate by coating a glass with dielectric medium. The reflection rate becomes maximum when the width of the dielectric medium d satisfies $d = (2l+1)\lambda/4$. When $\lambda = 2\pi/k$, this condition coincides with equation (62). Note that the parameter k in equation (62) is not exactly the wave number but it determines the profile of the magnetic fields (see equations (39), (40), and (41) for the definition of k). When the condition (62) is satisfied, the MHD waves propagating in the $+r$ direction are totally reflected by the density enhancement produced by the loop expansion. For the dipolar solution, the magnetic energy is transmitted to $r > R(t)$ because the density enhancement does not appear (see the right panels of Fig. 3 and Fig. 4).

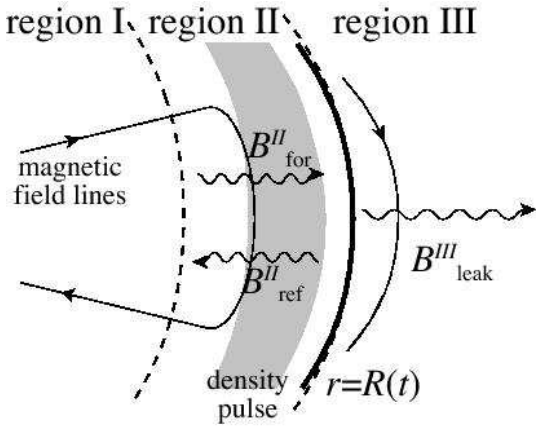

Figure 8. Schematic picture of the propagating waves. The forward wave $B_{\rm for}$ and the reflected waves $B_{\rm ref}$ propagate inside the loops. Solid curves show the loop top at $r = R(t)$, while the thin curves show the magnetic field lines. The superposition of these waves determines B_θ in region II. The leak wave $B_{\rm leak}$ appears ahead of the loop top in region III.

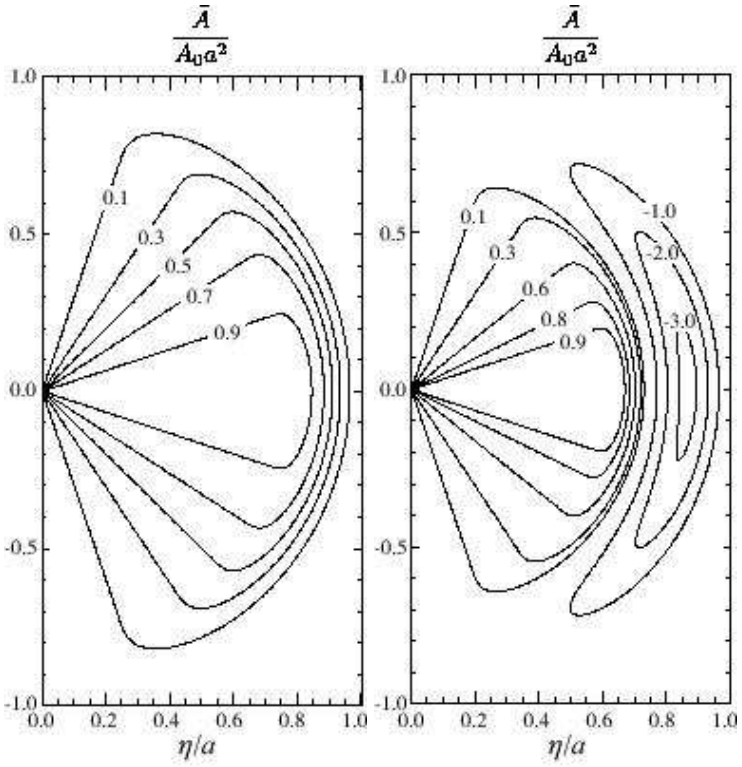

Figure 9. Contour plots of the flux function $\tilde{A}/(A_0a^2)$ of the shell solution for $k = \pi/[2(a-b)]$ (left panel) and $k = 3\pi/[4(a-b)]$ (right panel).

When $k > \pi/[2(a-b)]$, the magnetic shell recedes from $\eta \sim a$ to the region $b < \eta < a$, and a flux rope appears around $\eta = a$ ahead of the magnetic shell. Fig. 9 shows the contour plots of the magnetic flux $\tilde{A}$ of the shell solutions for $k = \pi/[2(a-b)]$ (left panel) and $k = 3\pi/[4(a-b)]$ (right panel).

3.4 Flux Rope Solutions

Flux rope solutions which include flux ropes inside the expanding magnetic loops are constructed by the flux function (42).

By substituting equation (42) into equation (32), the function Q can be written as

$$Q^I(\eta,\theta) = \sum_n \frac{Q_{0,n}}{(1-\eta^2)^{1+\frac{n}{4}}} \sin^n\theta, \tag{63}$$

$$Q^{II}(\eta,\theta) = \sum_n \frac{Q_{0,n}}{(1-\eta^2)^{1+\frac{n}{4}}} \Lambda^{\frac{n}{2}}(\eta) \sin^n\theta, \tag{64}$$

where $Q_{0,n}$ is a constant and subscripts I and II denote region I and region II, respectively. The pressure and density functions (i.e., P and D) can be obtained by substituting equations (42), (63), (64) into equations (31) and (33). The functions P and D obtained in region I and region II are given in appendix B.

The pressure and the gas density consist of three parts, the isotropic part P_0 and parts representing the interaction with the electromagnetic force by the poloidal and toroidal magnetic fields, P_A and P_Q (see equations (B1) and (B7) for the pressure and equations (B4) and (B10) for the gas density).

Fig. 10 shows the contour plots of the magnetic flux $\tilde{A}$ (left), the poloidal part of the pressure P_A (centre), and that of the gas density D_A (right) in $\eta/a - \theta$ plane. Fig. 11 shows contour plots of the toroidal magnetic field B_ϕ (left), the toroidal part of the pressure P_Q (centre), and that of the gas density D_Q (right) in $\eta/a - \theta$ plane. The parameters are taken to be $a = 0.8$, $b = 0.75a$, and $m = n = 4$ in both figures. The flux ropes exist behind the loop top (see the left panel of Fig. 10).

The magnetic fields in region I and II are explicitly given by

$$B^I_r = \frac{2A_0a^2}{r^2\sqrt{1-(r/t)^2}} \cos\theta, \tag{65}$$

$$B^I_\theta = -\frac{A_0a^2}{t^2[1-(r/t)^2]^{\frac{3}{2}}} \sin\theta, \tag{66}$$

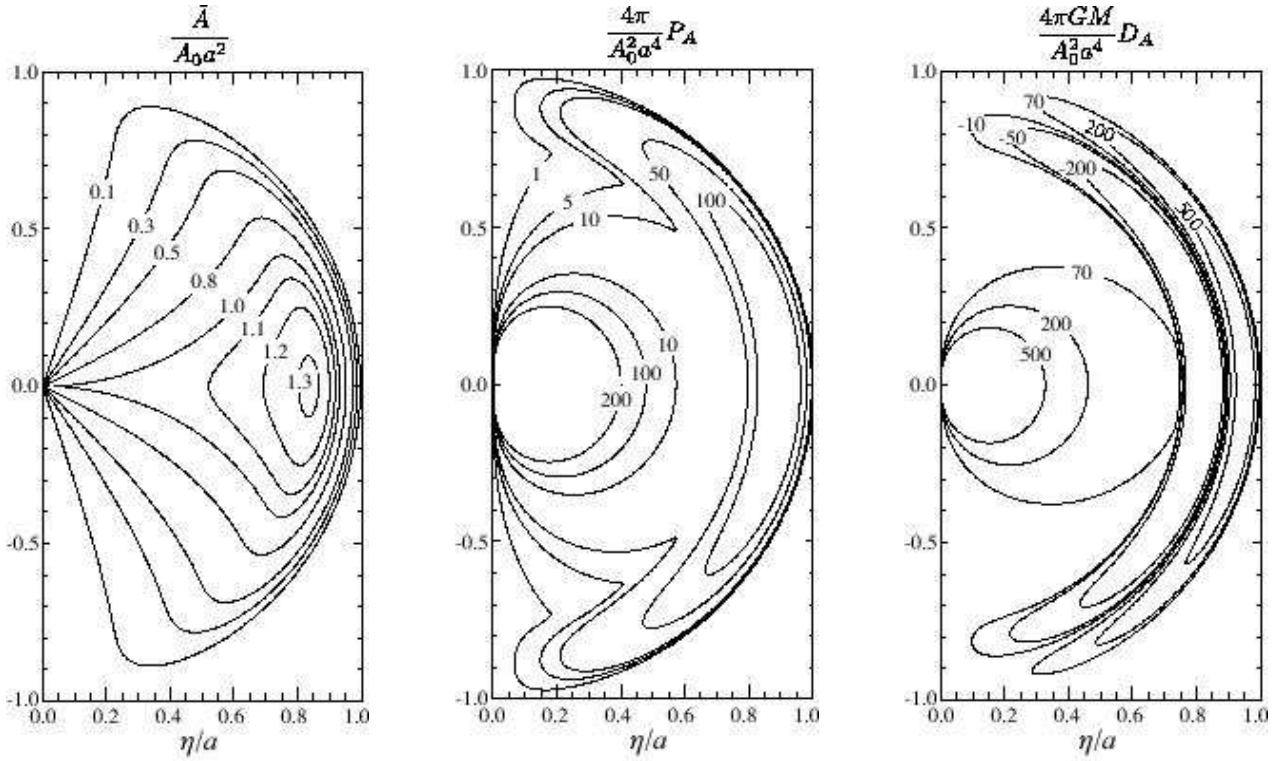

Figure 10. Contour plots of the magnetic flux $\tilde{A}$ (left), the poloidal part of the pressure P_A (centre), and that of the gas density D_A (right) for the flux rope solution in $\eta/a - \theta$ plane when $a = 0.8, b = 0.75a$.

$$B_\phi^I = \sum_n \frac{Q_{0,n}}{rt[1-(r/t)^2]^{1+\frac{n}{4}}} \sin^{n-1}\theta, \tag{67}$$

$$B_r^{II} = \frac{2A_0 a^2}{r^2} \frac{\Lambda\left(r/t\right)}{\sqrt{1-\left(r/t\right)^2}} \cos\theta, \tag{68}$$

$$B_\theta^{II} = \frac{A_0 a^2}{t^2} \frac{1}{\left[1-\left(r/t\right)^2\right]^{\frac{3}{2}}} \left\{ 4\frac{tk}{r}\left[1-\left(r/t\right)^2\right] \frac{\sin^3(T(r/t))\cos(T(r/t))}{\sin^4(T(a))} - \Lambda\left(r/t\right) \right\} \sin\theta, \tag{69}$$

$$B_\phi^{II} = \sum_n \frac{Q_{0,n}}{rt} \frac{\Lambda^{\frac{n}{2}}\left(r/t\right)}{\left[1-\left(r/t\right)^2\right]^{1+\frac{n}{4}}} \sin^{n-1}\theta. \tag{70}$$

Here the subscripts I and II denote the magnetic fields in region I and region II, respectively. Similarly to the dipolar and shell solutions, the parameter m represents the Fourier modes which specify where the magnetic twist is injected.

In the limit that $t \gg r$, the flux rope solution reduces to the dipolar solution given by equation (52), (53) and (54). In this limit, the magnetic field becomes stationary and radial.

Note that the field component B_r and B_θ are exactly zero but B_θ is not zero at $r = R(t)$ unless the condition (62) is satisfied. The electromagnetic energy is transmitted to $r > R(t)$ unless the condition (62) is satisfied as discussed in the previous subsection. When equation (62) is satisfied, the Poynting flux is totally reflected at $r = R(t)$ and the electromagnetic energy is not transmitted to $r \geqq R(t)$.

4 PHYSICAL PROPERTIES

Here we discuss physical properties of the three solutions we derived in § 3. In this section, we organize our discussion into four parts. First we consider the energetics. Second we show the shell and flux rope structures derived in § 3.3 and § 3.4 inside the magnetic loops. Third we study the relativistic effects, especially the role of the displacement current. Finally, we apply our solutions to SGR flares.

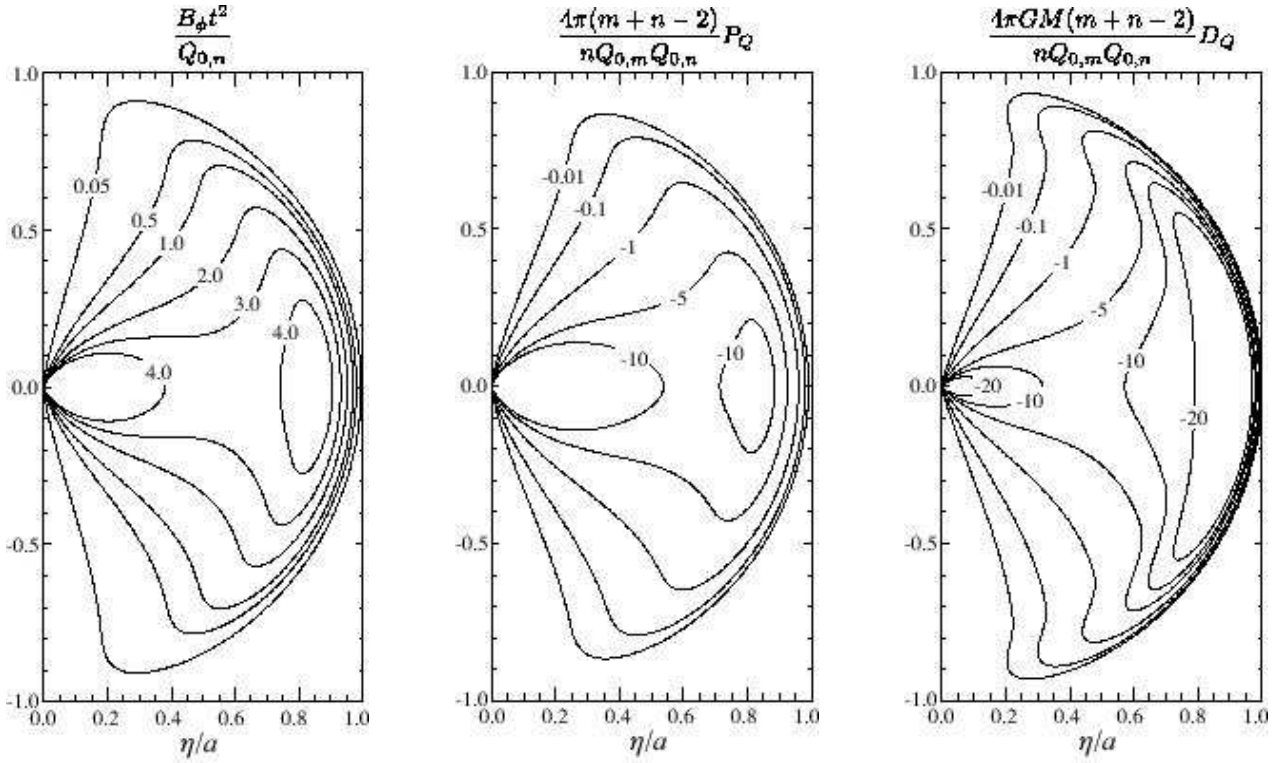

Figure 11. Contour plots of the toroidal magnetic field B_ϕ (left), the toroidal part of the pressure P_Q (centre), and that of the gas density D_Q (right) for the flux rope solution in $\eta/a - \theta$ plane when $a = 0.8, b = 0.75a$, and $n = m = 4$.

4.1 Energetics

First let us consider the dipolar solution without the toroidal magnetic field (i.e., $Q_{0,n} = 0$) for simplicity. Total energy $\mathcal{E}$ contained inside the expanding magnetic loops is given as

$$\mathcal{E} = K + U_{\rm in} + U_{\rm th} + U_{\rm E} + U_{\rm M} + W, \tag{71}$$

where

$$K = \int_V dV \rho\gamma^2, \tag{72}$$

$$U_{\rm in} = \int_V dV \frac{\Gamma}{\Gamma - 1}\gamma^2 v^2 p, \tag{73}$$

$$U_{\rm th} = \int_V dV \frac{p}{\Gamma - 1}, \tag{74}$$

$$U_{\rm E} = \int_V dV \frac{\boldsymbol{E}^2}{8\pi}, \tag{75}$$

$$U_{\rm M} = \int_V dV \frac{\boldsymbol{B}^2}{8\pi}, \tag{76}$$

$$W = -\int_V dV \frac{GM\gamma\rho}{r}, \tag{77}$$

are kinetic, thermal inertial, thermal, electric, magnetic, and gravitational potential energies, respectively. Since the solutions we derived describe the freely expanding magnetic loops, i.e., $Dv/Dt = 0$, the total kinetic energy K given by

$$K = \int_V \rho\gamma^2 dV = \int_0^a d\eta \int_0^{2\pi} d\theta \int_0^{\pi} d\phi \, \frac{\eta^2 D(\eta,\theta)}{\sqrt{1-\eta^2}} \sin\theta, \tag{78}$$

does not change with time. Here the total kinetic energy is integrated inside the spherical surface of $r = R(t)$. Other energies can be evaluated by carrying out the integration directly. The non-kinetic part of the total energy $\mathcal{E}' \equiv U_{\rm in} + U_{\rm th} + U_{\rm E} + U_{\rm M} + W$ contained inside $r = R(t)$ is then given as

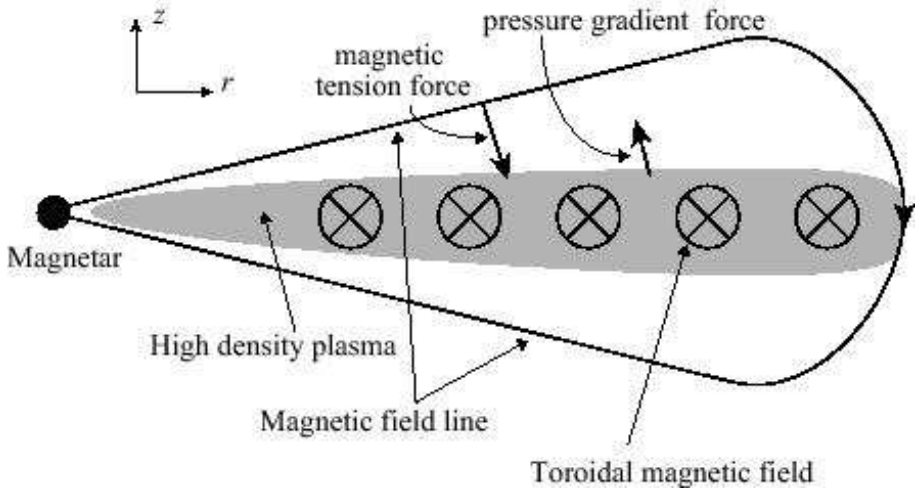

Figure 12. A schematic picture showing an expanding magnetic loop. Toroidal magnetic field is created inside the magnetic loop due to the twist injection from the surface of the magnetar. The magnetic pressure gradient force plus the pressure gradient force balances with the magnetic tension force by the poloidal magnetic field.

$$\mathcal{E}' = \frac{4A_0^2 a^3}{3t}. \tag{79}$$

Since the thermal, gravitational potential, and magnetic energies contain infinity due to the divergence of p, ρ, and B_r at $r = 0$ (see equations (45), (49), and (51), respectively), we renormalized the infinite parts of $U_{\rm th}$, $U_{\rm M}$, and W to zero (see Low 1982).

The non-kinetic part of the total energy $\mathcal{E}'$ depends on the amplitude of the poloidal magnetic field A_0, but is independent of the isotropic component (i.e., P_0 and D_0). The isotropic component does not contribute to the total energy because the thermal energy of the isotropic plasma cancels with that of the gravitational potential energy.

The energy $\mathcal{E}'$ diverges at $t = 0$ because we assumed a point mass at the origin. In magnetars, since the magnetar has a finite radius R_s, the self-similar expansion will take place when $r > r_0 > R_s$ and $t > t_0$. Let us denote the total energy and the non kinetic part of the total energy inside the spherical surface of $r_0 \equiv R(t_0)$ as $\mathcal{E}_0$ and $\mathcal{E}'_0$, respectively. The expansion takes place when $\mathcal{E}_0 > \mathcal{E}'_0$. Since the total kinetic energy $K = \mathcal{E}_0 - \mathcal{E}'_0$ does not change with time and $\mathcal{E}'(t)$ given in equation (79) decreases with time for the dipolar solution, $\mathcal{E}(t) = \mathcal{E}'(t) + K < \mathcal{E}'_0 + K = \mathcal{E}_0$. The released energy $\mathcal{E}_0 - \mathcal{E}(t)$ is carried away to $r > R(t)$. This can be confirmed by integrating the energy conservation equation inside the spherical surface $r = R(t)$ as

$$\int_{V(t)} \frac{\partial}{\partial t}\left[(\rho + 4p)\gamma^2 - p + \frac{\boldsymbol{E}^2 + \boldsymbol{B}^2}{8\pi} - \frac{GM\rho\gamma}{r}\right] d^3\boldsymbol{r} + \int_{V(t)} \nabla\cdot\left[(\rho + 4p)\gamma^2\boldsymbol{v} + \frac{\boldsymbol{E}\times\boldsymbol{B}}{4\pi} - \frac{GM\rho\gamma}{r}\boldsymbol{v}\right] d^3\boldsymbol{r} = 0. \tag{80}$$

Since this integration is cumbersome, we do not show the details of the calculation. We have to point out that the integration with the volume V cannot be exchanged with the time derivative in the first term since the volume V changes with time.

Next let us consider the case $Q_{0,n} \neq 0$. Since the integration of equations (72)-(77) is complex, we evaluate the total energy inside the closed boundary by a different method. Note that equation (36), which represents equations of motion in the self-similar space, indicates that the self-similar equations we derived are closely related to the static relativistic MHD solutions except the existence of the thermal inertial term and the electric field. We can derive the virial theorem for the relativistic self-similar MHD (see appendix C);

$$3(\Gamma - 1)U_{\rm th} + U_{\rm in} + U_{\rm M} + U_{\rm E} + W = \mathcal{H} + \mathcal{S}, \tag{81}$$

where

$$\mathcal{H} = \int p\boldsymbol{r}\cdot d\boldsymbol{\mathcal{A}} - \frac{1}{8\pi}\int \left\{2\left[(\boldsymbol{r}\cdot\boldsymbol{E})(\boldsymbol{E}\cdot d\boldsymbol{\mathcal{A}}) + (\boldsymbol{r}\cdot\boldsymbol{B})(\boldsymbol{B}\cdot d\boldsymbol{\mathcal{A}})\right] - (\boldsymbol{E}^2 + \boldsymbol{B}^2)(\boldsymbol{r}\cdot d\boldsymbol{\mathcal{A}})\right\}, \tag{82}$$

and

$$\mathcal{S} = \int dV \frac{\partial}{\partial t}\left(\boldsymbol{r}\cdot\frac{\boldsymbol{E}\times\boldsymbol{B}}{4\pi}\right). \tag{83}$$

Here $\boldsymbol{\mathcal{A}}$ is the surface enclosing the volume V. The non-kinetic part of the total energy $\mathcal{E}'$ can be written from equation (81) as

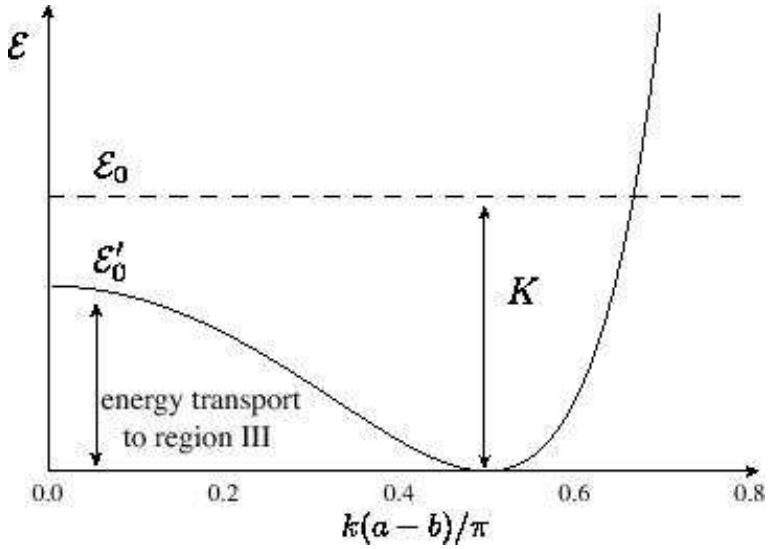

Figure 13. k dependence of the non kinetic part of the total energy $\mathcal{E}'$ (solid curve) for the shell and flux rope solutions.

$$\mathcal{E}' = -(3\Gamma - 4)U_{\rm th} + \mathcal{H} + \mathcal{S}. \tag{84}$$

We can evaluate $\mathcal{E}'$ inside the expanding spherical surface of $r = R(t)$ by using the fact that $p = \rho = B_r = B_\phi = 0$ at $r = R(t)$ as

$$\mathcal{E}' = \begin{cases} \dfrac{4A_0^2 a^3}{3t}, & \text{(dipolar solution)}, \\ \dfrac{16A_0^2 a^5 k^2 (1-a^2)\cot^2 T(a)}{3t}, & \text{(shell solution)}, \\ \dfrac{16A_0^2 a^5 k^2 \cot^2 T(a)}{3t}, & \text{(flux rope solution)}, \end{cases} \tag{85}$$

In all solutions, the non-kinetic part of the total energy does not depend on the toroidal magnetic field because the toroidal magnetic field does not change the dynamics of the expanding magnetic loops in the self-similar stage. This can be understood from the fact that when we take $Q_{0,n} = 0$, the solutions we derived satisfy equations (31), (32) and (33) without any modification on the poloidal magnetic field. To understand this reason, let us consider the equation of motion in the θ direction. Since $\boldsymbol{v} = v\boldsymbol{e}_r$, the force balance should be attained in the θ direction (see Fig. 12). The pressure P_Q is smaller for larger toroidal magnetic fields because P_Q is proportional to $-Q_{0,n}^2$ (see equations (46) for the dipolar solution, (A4) and (A11) for the shell solution, and (B3) and (B9) for the flux rope solution). For larger toroidal magnetic fields, the magnetic pressure gradient force by the toroidal magnetic field balances with the magnetic tension force from the poloidal magnetic field. As a result, the existence of the toroidal magnetic field modifies the plasma distribution, but does not change the dynamics.

Fig. 13 shows the k dependence of $\mathcal{E}_0'$ for the shell and flux rope solutions (note that both solutions have the same k dependence). When the condition (62) is satisfied, the total energy contained inside the magnetic loops is equal to K and conserved for the shell and flux rope solutions because the energy flux is zero at $r = R(t)$. When (62) is not satisfied, the total energy is larger than K by $\mathcal{E}'$ (see equation (62)). The excess energy is carried away to the region III ($r > R(t)$) to attain the free expansion, i.e., $Dv/Dt = 0$.

4.2 Shell and Flux Rope Structures

Let us examine the density and pressure distribution for the shell solution derived in § 3.3. We define the density and pressure enhancements as

$$\Delta P_A = \left[\frac{2\pi\eta^4}{A_0^2 a^4 \sin^2\theta}\right] P_A, \tag{86}$$

$$\Delta D_A = \left[\frac{\pi G M \eta^3 (1-\eta^2)}{2A_0^2 a^4 \sin^2\theta}\right] D_A, \tag{87}$$

$$\Delta P_Q = \left[\frac{4\pi(m+n-2)\eta^2(1-\eta^2)}{nQ_{0,m}Q_{0,n}\sin^{m+n-2}\theta}\right] P_Q, \tag{88}$$

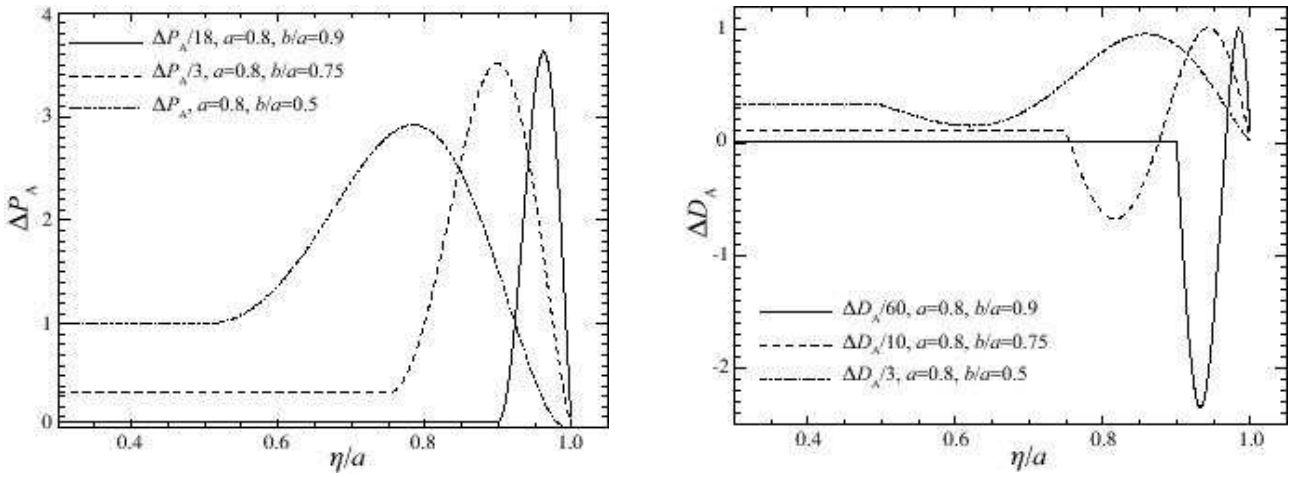

Figure 14. The pressure enhancement ΔP_A (left) and the density enhancement ΔD_A (right) for the shell solution are shown as a function of η/a. Solid curve is for $b = 9a/10$, while the dashed and dot-dashed ones are for $b = 3a/4$ and $b = a/2$, respectively. Other parameters are fixed at $a = 0.8$ and $k = \pi/[4(a-b)]$.

$$\Delta D_Q = \left[\frac{2\pi GM(m+n-2)\eta(1-\eta^2)^2}{nQ_{0,m}Q_{0,n}\sin^{m+n-2}\theta}\right] D_Q, \tag{89}$$

These functions are normalized to be unity in region I, where the poloidal magnetic field lines are radial for the shell solution. In Fig. 14, the pressure and density enhancements, ΔP_A and ΔD_A are plotted for $b = a/2,\ 3a/4,\ 9a/10$ when $a = 0.8$ and $k = \pi/[4(a-b)]$. In all three cases, the pressure and density pulses appear at the top of the magnetic loops. Their amplitudes are larger for a thinner shell. The peak of the pressure enhancement appears behind that of the density enhancement. This structure comes from the requirement for the force balance with the gravity. As mentioned in § 4.1, this relativistic self-similar solution is similar to the static solution in which the force balance is attained. As plasma is swept up into the shell, the density increases inside the shell. To support the gravity by this excess density, the pressure gradient appears behind the density enhancement. The density decrease behind the pressure enhancement also comes from the requirement for the force balance. Since the decrease of the density enables the buoyancy force to push the plasma in the radial direction, this buoyancy force maintains the pressure pulse. These structures are identical to those in non-relativistic solution (Low 1982).

Fig. 15 plots ΔP_Q and ΔD_Q for $b = a/2,\ 3a/4,\ 9a/10$ when $a = 0.8$ and $k = \pi/[4(a-b)]$. As mentioned in § 3, the Lorentz force exerted by the toroidal magnetic fields always reduces the pressure. A local minimum of the density enhancement ΔD_Q locates behind a local maximum of $d\Delta P_Q/d\eta$. This structure also comes from the force balance. Pressure gradient force balances with the buoyancy force in the rarefied region.

Next we examine the structure of the flux rope solution derived in § 3.4. We define the normalized toroidal magnetic field strength as

$$\Delta B_\phi(\eta) = \frac{B_\phi t^2}{Q_{0,n}\sin^{n-1}\theta}. \tag{90}$$

Solid curve in Fig. 16 shows ΔB_ϕ as a function of η for $b = 0.95a$, while the dash and dot-dashed ones show that for $b = 0.8a$ and $b = 0.65a$, respectively. Other parameters are fixed at $a = 0.8$ and $k = \pi/[4(a-b)]$. The toroidal magnetic field has a peak inside the flux rope. Its amplitude is larger for a larger a and a thinner shell. The shell structure also appears behind the loop top (see Fig. 10 and 11). Solid curve in Fig. 17 shows ΔB_ϕ^2, which corresponds to the magnetic pressure by the toroidal magnetic field, as a function of η for $a = 0.8$, $b = 0.95a$, and $k = \pi/[4(a-b)]$. Dashed and dot-dashed curves show ΔP_Q and ΔD_Q, respectively. Plasma density decreases inside the shell. The decrement of the plasma density leads to the buoyancy force which balances with the pressure gradient force in front of the shell. Behind the shell, the pressure gradient force balances with that of the magnetic pressure. This effect is more prominent for the flux rope solution than for the shell solution since the magnetic pressure is enhanced inside the flux rope.

4.3 The Role of the Displacement Current

We showed that P_Q is always negative. On the other hand, P_A can have either positive or negative values. In this subsection, we obtain the condition for $P_A < 0$.

First let us consider the dipolar solution derived in § 3.2. The condition that P_A given by equation (45) is positive in $0 \leqq \eta \leqq a$ is given by

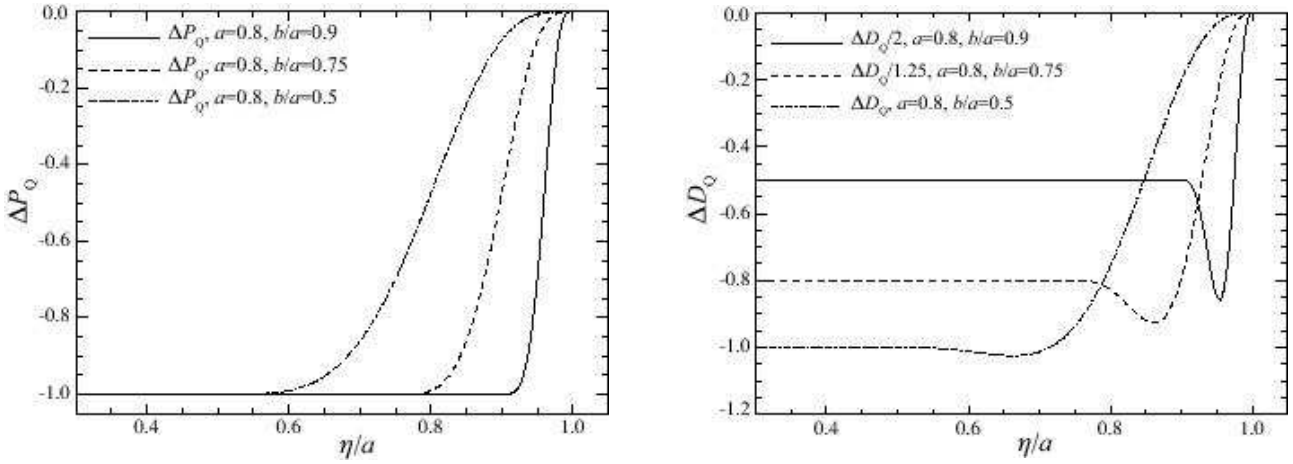

Figure 15. The pressure decrement ΔP_Q (left) and the density decrement ΔD_Q (right) by the azimuthal field are shown as a function of η/a for the shell solution. Solid curve is for $b = 9a/10$, while dashed and dot-dashed curves are for $b = 3a/4$ and $b = a/2$, respectively. Other parameters are fixed at $a = 0.8$ and $k = \pi/[4(a-b)]$.

$$2a^2 - 3a^2\eta^2 - \eta^4 + 2\eta^6 \geqq 0. \tag{91}$$

The critical value a_* for $P_A > 0$ in $0 \leqq \eta \leqq a$ is

$$a_* = \frac{\sqrt{69 + 11\sqrt{33}}}{12} \simeq 0.958. \tag{92}$$

When $a > a_*$, P_A has negative values in the domain $0 \leqq \eta \leqq a$. Since a denotes the expansion speed of the magnetic loops at $r = R(t)$, the above condition indicates that P_A can be negative for faster expansion.

Next let us calculate the azimuthal component of the current density,

$$j_\phi = j_{\rm rot} + j_{\rm disp}, \tag{93}$$

where

$$j_{\rm rot} \equiv \frac{(\nabla \times \boldsymbol{B})_\phi}{4\pi} = \frac{A_0 a^2}{4\pi r^3} \frac{2a^2 - 5a^2\eta^2 + 5\eta^4 - 2\eta^6}{(1-\eta^2)^{\frac{5}{2}}} \sin\theta, \tag{94}$$

$$j_{\rm disp} \equiv -\frac{1}{4\pi}\frac{\partial E_\phi}{\partial t} = -\frac{A_0 a^2}{4\pi r^3} \frac{\eta^4\left(6 - 3a^2 - 5\eta^2 + 2\eta^4\right)}{(1-\eta^2)^{\frac{5}{2}}} \sin\theta, \tag{95}$$

and

$$j_\phi = \frac{A_0 a^2}{4\pi r^3} \frac{2a^2 - 3a^2\eta^2 - \eta^4 + 2\eta^6}{(1-\eta^2)^{\frac{3}{2}}} \sin\theta. \tag{96}$$

The current $j_{\rm rot}$ is always positive, while $j_{\rm disp}$ has negative values for a larger a in $0 \leqq \eta \leqq a$. The displacement current $j_{\rm disp}$ cannot be ignored for a larger a and it reduces the azimuthal current j_ϕ. Thus the current j_ϕ changes its sign for a larger a. Remember that the pressure P is determined by the θ component of the equation of motion given by

$$(-\nabla p + \boldsymbol{j} \times \boldsymbol{B} + \rho_e \boldsymbol{E})_\theta = 0. \tag{97}$$

According to the definition of P_A and P_Q, the poloidal component of equation (97) is given by

$$\frac{1}{t^4 r}\frac{\partial P_A}{\partial \theta} = j_\phi B_r. \tag{98}$$

Since both $\partial P_A/\partial\theta$ and $j_\phi B_r$ depend on θ by $\sin\theta\cos\theta$, and $B_r/\cos\theta$ is positive, the sign of P_A is determined by that of $j_\phi/\sin\theta$. Thus P_A can be negative when the displacement current $j_{\rm disp}$ dominates the current $j_{\rm rot}$. The condition that $j_\phi \leqq 0$ coincides with the condition that $P_A \leqq 0$ (i.e. $a \geqq a_*$, where a_* is given by equation (92)).

Next let us consider the shell and flux rope solutions. Since these solutions are more complex, the equation $P_A = 0$ is solved numerically. Instead of using parameters a and b, we introduce the following parameters,

$$V_{\rm max} = a, \tag{99}$$

$$\Delta = \frac{a-b}{a}. \tag{100}$$

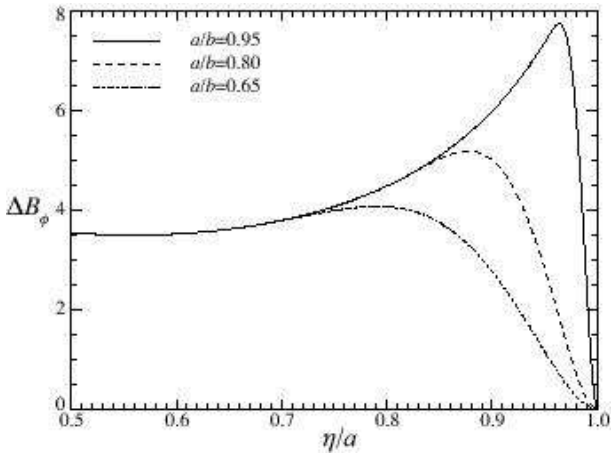

Figure 16. Distribution of ΔB_ϕ for the flux rope solution as a function of η/a for $a = 0.8$. Solid curve is for $b/a = 0.95$, while dashed and dot-dashed ones are for $b/a = 0.8$ and $b/a = 0.65$, respectively.

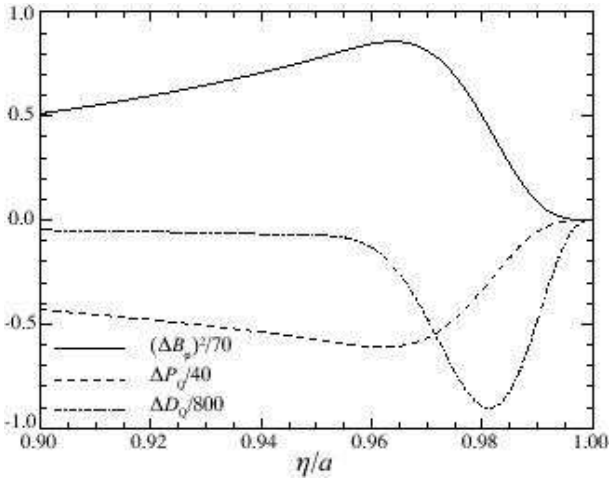

Figure 17. Distribution of ΔB_ϕ^2 for the flux rope solution as a function of η/a for $a = 0.8$ and $b/a = 0.95$ (solid curve). Dashed and dot-dashed ones denote ΔP_Q and ΔD_Q, respectively.

These parameters denote the maximum speed of the expanding loops and thickness of the shell behind the loop top, respectively. Fig. 18 is a diagram showing whether the solution that $P_A = 0$ exists for the shell and flux rope solutions in the parameter space of $V_{\max}$ and Δ for $k = \pi/[4(a-b)]$. Solutions where $P_A = 0$ exist in the shaded area for the shell solution and in the grey area for the flux rope solution. Similarly to the dipolar solution, the effect of the displacement current is more prominent for a larger $V_{\max}$. Generally, P_A is smaller for a larger $V_{\max}$ and thicker shells in parallel that the displacement current becomes important for larger $V_{\max}$ and Δ. For the flux rope solution, the displacement current is important not only in region II but in region I (right bottom region in Fig. 18). In this case, P_A is negative for $b \geqq 0.817$.

4.4 Application to SGR Explosions

SGR flares can be triggered by energy injection into magnetic loops at the surface of a strongly magnetized neutron star (e.g., Lyutikov 2006). When sufficiently large energy is injected, the magnetic loops will become dynamically unstable, and expand relativistically. Magnetic energy release in the expanding magnetic loops can be the origin of SGR flares. The expanding magnetic loops will also produce magnetosonic waves propagating ahead of the loops. High energy particles can be produced in the magnetic reconnection inside the loops, and in shock fronts formed ahead of the loops.

In this paper, we did not solve the structure of the region ahead of the magnetic loops ($r > R(t)$). When the outer region is a vacuum, electromagnetic waves will be emitted from the boundary at $r = R(t)$. When the plasma density is much larger than the Goldreich-Julian density (Goldreich & Julian 1969) and the wave frequency is much smaller than the plasma frequency, the outer plasma can be studied by using MHD equations. It will be our future work to connect the self-similar solutions inside $r = R(t)$ and the solutions in $r \geqq R(t)$.

Now let us estimate the energy for the SGR explosion based on the self-similar solutions. Let us take the field strength to be 10^{15} Gauss (Kouveliotou et al. 1998; Ibrahim et al. 2002; Ibrahim et al. 2003) at the stellar radius $R_s = 10^6$ cm. This leads to

$$\frac{2A_0 a^2}{R_s^2} = 10^{15} \text{ Gauss}. \tag{101}$$

By assuming that the self-similar expansion begins when $t_0 = R_s/a$, the released energy from the expanding magnetic loops can be estimated from equation (85) as

$$\mathcal{E}' = \begin{cases} 6 \times 10^{46} \text{ erg}, & \text{(dipolar solution)}, \\ 2 \times 10^{47} \Delta^{-2} \text{ erg}, & \text{(shell solution)}, \\ 8 \times 10^{47} \Delta^{-2} \text{ erg}, & \text{(flux rope solution)}. \end{cases} \tag{102}$$

Here we take $a = V_{\max} \simeq 0.9$ and $k = \pi/[4(a-b)]$. These results agree with the observed energy of SGR giant flares (Hurley et al. 2005; Palmer et al. 2005; Terasawa et al. 2005). Note that the total energy contained in the expanding magnetic loops is more energetic for thinner shells. The non-kinetic part of the total energy $\mathcal{E}'$ is inversely proportional to the square of the shell thickness. When some fraction of the kinetic energy K is converted to the electromagnetic energy, the released energy can be larger than that estimated by equation (102).

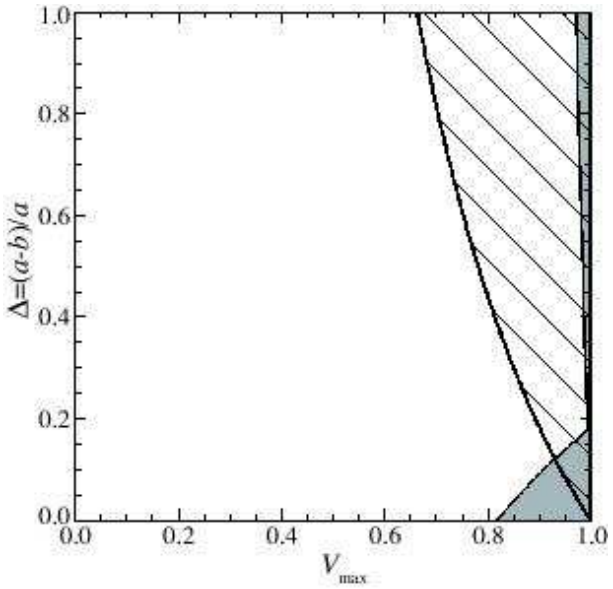

Figure 18. The diagram showing where the solution $P_A = 0$ exists in the parameter space $V_{\max}$ and $\Delta = (a-b)/a$ when $k = \pi/[4(a-b)]$ for the shell solution (the shaded area) and for the flux the rope solution (grey area).

5 SUMMARY & DISCUSSIONS

By extending the self-similar solutions derived by Low (1982), we derived self-similar solutions of relativistically expanding magnetic loops taking into account the toroidal magnetic fields. The dipolar solution derived in § 3.2 gives us an insight into the relativistic expansion of the magnetic loops because of its simplicity. However, the shell and flux rope solutions derived in § 3.3, 3.4 have more physically interesting properties such as an enhanced magnetic pressure at the shells and flux rope structures. Such configurations might be more probable for SGR flares.

The equations of motion in the self-similar stage are similar to those of the static equilibrium state except the existence of the relativistic thermal inertial term and the electric field. This fact allows us to evaluate the non-kinetic part of the total energy in the magnetic loops by using the virial theorem. The magnetic loops with shell or flux rope structures carry more energy than the simple dipole solution. The energy is comparable to the observed energy of the SGR giant flares.

In relativistically expanding magnetic loops, the effect of the displacement current becomes important. In dipolar solution, the displacement current becomes larger than the real current $\nabla \times \boldsymbol{B}/(4\pi)$ for faster expansion speed ($V_{\max} > a_*$). This effect reduces the toroidal current and weakens the magnetic tension force. To balance the reduced magnetic tension force, the pressure decreases.

We found that the energy is transferred to $r > R(t)$ in dipolar solutions. In the shell and flux rope solutions, the energy is transferred to $r > R(t)$ unless condition (62) is satisfied. The condition can be interpreted as that for the total reflection of the MHD waves in the shell. Dipolar solutions always have leakage (transmission of Poynting flux to the region $r \geqq R(t)$) because $B_\theta \neq 0$ at $r = R(t)$. The shell and flux rope solutions have perfectly reflecting solutions in which the total energy in $r < R(t)$ is conserved. It means that the solutions are energy eigenstates of the system. The eigenstates can be obtained by adjusting the parameter k.

In this paper, we obtained solutions for freely expanding magnetic loops, i.e., $Dv/Dt = 0$. We assumed that the magnetic loops have sufficiently large energy to drive the expansion. When the flux function $\tilde{A}$ increases with time, the toroidal magnetic fields will also increase with time. The toroidal magnetic fields will then affect the dynamics through the magnetic pressure. Such solutions can describe the accelerating magnetic loops.

Magnetic fields can be expressed as the sum of the Fourier modes in the polar angle. The modes and their amplitudes should be determined at the boundary where the magnetic twist is injected on the surface of the star. It is not shown but we can construct more complex solutions that the poloidal magnetic fields are expressed by the sum of the Fourier modes, i.e., $\tilde{A} \propto \sin^n \theta$. In actual explosion, the opening angle of the expanding magnetic loops depends on the location at which the magnetic twist is injected on the surface of the central star. Such a solution may be expressed as the sum of the Fourier modes for the poloidal and toroidal magnetic fields. We should note that SGR flares are not necessarily axisymmetric. Models including the non-axisymmetrically expanding magnetic loops will be a subject of future works.

ACKNOWLEDGMENTS

We are grateful to the anonymous referee for constructive comments improving the paper. Fruitful discussions with Tomoyuki Hanawa, Akira Mizuta, and Tomohisa Kawashima at Chiba University are greatly appreciated. This work was supported by the Grants-in-Aid for Scientific Research of Ministry of Education, Culture, Sports, Science, and Technology (RM:20340040).

REFERENCES

Asano E., 2007, PhD. thesis, Chiba Univ.
Asano E., Uchida T., Matsumoto R., 2005, PASJ, 57, 409
Chandrasekhar S., Fermi E., 1953, ApJ, 118, 116
Goldreich P., Julian W. H., 1969, ApJ, 157, 869
Hurley K., Boggs S. E., Smith D. M., Duncan R. C., Lin R., Zoglauer A., Krucker S., Hurford G., Hudson H., Wigger C., Hajdas W., Thompson C., Mitrofanov I., Sanin A., Boynton W., Fellows C., von Kienlin A., Lichti G., Rau A., Cline T., 2005, Nature, 434, 1098
Ibrahim A. I., Safi-Harb S., Swank J. H., Parke W., Zane S., Turolla R., 2002, ApJ, 574, L51
Ibrahim A. I., Swank J. H., Parke W., 2003, ApJ, 584, L17
Komissarov S. S., 2002, MNRAS, 336, 759
—, 2006, MNRAS, 367, 19
Kouveliotou C., Dieters S., Strohmayer T., van Paradijs J., Fishman G. J., Meegan C. A., Hurley K., Kommers J., Smith I., Frail D., Murakami T., 1998, Nature, 393, 235
Landau L. D., Lifshitz E. M., 1975, The classical theory of fields. 4th edition: Volume 2 (Course of theoretical physics), p. 90, Betterworth-Heinemann
Low B. C., 1982, ApJ, 261, 351
—, 1984, ApJ, 281, 392
Lyutikov M., 2002, Physics of Fluids, 14, 963
—, 2006, MNRAS, 367, 1594
Lyutikov M., Blandford R., 2003, astro-ph/0312347
Mereghetti S., 2008, A&A Rev., 15, 225
Palmer D. M., Barthelmy S., Gehrels N., Kippen R. M., Cayton T., Kouveliotou C., Eichler D., Wijers R. A. M. J., Woods P. M., Granot J., Lyubarsky Y. E., Ramirez-Ruiz E., Barbier L., Chester M., Cummings J., Fenimore E. E., Finger M. H., Gaensler B. M., Hullinger D., Krimm H., Markwardt C. B., Nousek J. A., Parsons A., Patel S., Sakamoto T., Sato G., Suzuki M., Tueller J., 2005, Nature, 434, 1107
Prendergast K. H., 2005, MNRAS, 359, 725
Spitkovsky A., 2005, in KITP Program: Physics of Astrophysical outflows and Accretion disks (http://online.kitp.ucsb.edu/online/)
—, 2006, ApJ, 648, L51
Stone J. M., Hawley J. F., Evans C. R., Norman M. L., 1992, ApJ, 388, 415
Terasawa T., Tanaka Y. T., Takei Y., Kawai N., Yoshida A., Nomoto K., Yoshikawa I., Saito Y., Kasaba Y., Takashima T., Mukai T., Noda H., Murakami T., Watanabe K., Muraki Y., Yokoyama T., Hoshino M., 2005, Nature, 434, 1110
Thompson C., Duncan R. C., 2001, ApJ, 561, 980
Uchida T., 1997, Phys. Rev. E, 56, 2181
Woods P. M., Kouveliotou C., Göğüş E., Finger M. H., Swank J., Smith D. A., Hurley K., Thompson C., 2001, ApJ, 552, 748
Woods P. M., Thompson C., 2006, in Lewin W., van der Klis M., eds, Cambridge Astrophys. Ser. Vol. 39, p. 547, Compact stellar X-ray sources, Cambridge Univ. Press, Cambridge

APPENDIX A: CONSTRUCTION OF THE SHELL SOLUTIONS

The functions Q and P in region I are given by

$$Q^I(\eta,\theta) = \sum_n \frac{Q_{0,n}}{1-\eta^2}\sin^n\theta, \tag{A1}$$

$$P^I(\eta,\theta) = P_0(\eta) + P_A^I(\eta,\theta) + P_Q^I(\eta,\theta), \tag{A2}$$

where P_A^I and P_Q^I are given by

$$P_A^I(\eta,\theta) = \frac{A_0^2 a^4}{2\pi\eta^4}\sin^2\theta, \tag{A3}$$

$$P_Q^I(\eta,\theta) = \begin{cases} -\sum\limits_{m+n\neq 2} \frac{nQ_{0,m}Q_{0,n}}{4\pi(m+n-2)\eta^2(1-\eta^2)}\sin^{m+n-2}\theta, & \text{for } m+n\neq 2, \\ -\sum\limits_{m+n=2} \frac{nQ_{0,m}Q_{0,m}}{4\pi\eta^2(1-\eta^2)}\log(\sin\theta), & \text{for } m+n=2. \end{cases} \tag{A4}$$

The function D in region I is given by

$$D^I(\eta,\theta) = D_0(\eta) + D_A^I(\eta,\theta) + D_Q^I(\eta,\theta), \tag{A5}$$

where D_A^I and D_Q^I are given by

$$D_A^I(\eta,\theta) = \frac{2A_0^2 a^4}{\pi GM\eta^3(1-\eta^2)}\sin^2\theta, \tag{A6}$$

$$D_Q^I(\eta,\theta) = \begin{cases} -\sum\limits_{m+n\neq 2} \frac{nQ_{0,m}Q_{0,n}}{2\pi GM(m+n-2)\eta(1-\eta^2)^2}\sin^{m+n-2}\theta, & \text{for } m+n\neq 2, \\ -\sum\limits_{m+n=2} \frac{nQ_{0,m}Q_{0,m}}{2\pi GM\eta(1-\eta^2)^2}\log(\sin\theta), & \text{for } m+n=2. \end{cases} \tag{A7}$$

The functions Q and P in region II are given by

$$Q^{II}(\eta,\theta) = \sum_n \frac{Q_{0,n}}{1-\eta^2}\Lambda^{\frac{n}{2}}(\eta)\sin^n\theta, \tag{A8}$$

$$P^{II}(\eta,\theta) = P_0(\eta) + P_A^{II}(\eta,\theta) + P_Q^{II}(\eta,\theta), \tag{A9}$$

where P_A^{II} and P_Q^{II} are given by

$$P_A^{II}(\eta,\theta) = \frac{A_0^2 a^4}{2\pi\eta^4}\Lambda(\eta)\left\{1 - \frac{\sin^2 T(\eta)}{\sin^4 T(a)}\left[\sin^2 T(\eta) + 4k\eta^3\sin T(\eta)\cos T(\eta) - 2k^2\eta^2(1-\eta^2)\left(3-4\sin^2 T(\eta)\right)\right]\right\}\sin^2\theta, \tag{A10}$$

$$P_Q^{II}(\eta,\theta) = \begin{cases} -\sum\limits_{m+n\neq 2} \frac{nQ_{0,m}Q_{0,n}\Lambda^{\frac{(m+n)}{2}}(\eta)}{4\pi(m+n-2)\eta^2(1-\eta^2)}\sin^{m+n-2}\theta, & \text{for } m+n\neq 2, \\ -\sum\limits_{m+n=2} \frac{nQ_{0,m}Q_{0,n}\Lambda(\eta)}{4\pi\eta^2(1-\eta^2)}\log(\sin\theta), & \text{for } m+n=2. \end{cases} \tag{A11}$$

The function D^{II} is given by

$$D^{II}(\eta,\theta) = D_0(\eta) + D_A^{II}(\eta,\theta) + D_Q^{II}(\eta,\theta), \tag{A12}$$

where D_A^{II} and D_Q^{II} are given by

$$D_A^{II}(\eta,\theta) = \frac{2A_0^2 a^4}{\pi GM\eta^3(1-\eta^2)}\Lambda(\eta)\left[1 - \frac{\sin^4 T(\eta)}{\sin^4 T(a)}\Xi(\eta)\right]\sin^2\theta, \tag{A13}$$

$$D_Q^{II}(\eta,\theta) = \begin{cases} -\sum\limits_{m+n\neq 2} \frac{nQ_{0,m}Q_{0,n}\Lambda^{\frac{m+n-2}{2}}(\eta)}{2\pi GM(m+n-2)\eta(1-\eta^2)^2}\left\{1 - \frac{\sin^4 T(\eta)}{\sin^4 T(a)}\left[1 - 2k\eta(1-\eta^2)\cot T(\eta)\right]\right\}\sin^{m+n-2}\theta, \\ \qquad\qquad \text{for } m+n\neq 2, \\ -\sum\limits_{m+n=2} \frac{nQ_{0,m}Q_{0,n}}{2\pi GM\eta(1-\eta^2)^2}\left\{\log(\sin\theta) - \frac{\sin^4 T(\eta)}{\sin^4 T(a)}\left[\log(\sin\theta) + k\eta(1-\eta^2)\cot T(\eta)(1-2\log(\sin\theta))\right]\right\}, \\ \qquad\qquad \text{for } m+n=2. \end{cases} \tag{A14}$$

Here $\Xi(\eta)$ is a function of η given by

$$\Xi(\eta) = 1 - k\eta(1+\eta^2)(1-3\eta^2)\cot T(\eta) + k^2\eta^2(1-\eta^2)(1+3\eta^2)\left[1-3\cot^2 T(\eta)\right] + k^3\eta^3(1-\eta^2)^2\left[3\cot^3 T(\eta) - 5\cot T(\eta)\right]. \tag{A15}$$

$P_0(\eta)$ is an arbitrary function of η and is related to the function $D_0(\eta)$ through equation (48).

APPENDIX B: CONSTRUCTION OF THE FLUX ROPE SOLUTIONS

The function P in region I is given by

$$P^I(\eta,\theta) = P_0(\eta) + P_A^I(\eta,\theta) + P_Q^I(\eta,\theta), \tag{B1}$$

where P_A^I and P_Q^I are

$$P_A^I(\eta,\theta) = \frac{A_0^2 a^4}{4\pi\eta^4}\frac{2-3\eta^2}{(1-\eta^2)^2}\sin^2\theta, \tag{B2}$$

$$P_Q^I(\eta,\theta) = \begin{cases} -\displaystyle\sum_{m+n\neq 2} \frac{nQ_{0,m}Q_{0,n}}{4\pi(m+n-2)}\frac{\sin^{m+n-2}\theta}{\eta^2(1-\eta^2)^{1+(m+n)/4}}, & \text{for } m+n\neq 2, \\ -\displaystyle\sum_{m+n=2} \frac{nQ_{0,m}Q_{0,n}}{4\pi}\frac{\log(\sin\theta)}{\eta^2(1-\eta^2)^{\frac{3}{2}}}, & \text{for } m+n=2. \end{cases} \tag{B3}$$

The function D in region I is given by

$$D^I(\eta,\theta) = D_0(\eta) + D_A^I(\eta,\theta) + D_Q^I(\eta,\theta), \tag{B4}$$

where D_A^I and D_Q^I are

$$D_A^I(\eta,\theta) = \frac{A_0^2 a^4}{4\pi GM\eta^3}\frac{8-12\eta^2+3\eta^4}{(1-\eta^2)^3}\sin^2\theta, \tag{B5}$$

$$D_Q^I(\eta,\theta) = \begin{cases} -\displaystyle\sum_{m+n\neq 2} \frac{nQ_{0,m}Q_{0,n}}{4\pi GM(m+n-2)}\frac{2-\eta^2}{\eta(1-\eta^2)^{2+(m+n)/4}}\sin^{m+n-2}\theta, & \text{for } m+n\neq 2, \\ -\displaystyle\sum_{m+n=2} \frac{nQ_{0,m}Q_{0,n}}{8\pi GM}\frac{\eta^2+2(2-\eta^2)\log(\sin\theta)}{\eta(1-\eta^2)^{\frac{5}{2}}}, & \text{for } m+n=2. \end{cases} \tag{B6}$$

The function P in region II is described as

$$P^{II}(\eta,\theta) = P_0(\eta) + P_A^{II}(\eta,\theta) + P_Q^{II}(\eta,\theta), \tag{B7}$$

where P_A^{II} and P_Q^{II} are

$$P_A^{II} = \frac{A_0^2 a^4}{4\pi\eta^4}\Lambda(\eta)\left[\frac{2-3\eta^2}{(1-\eta^2)^2}\Lambda(\eta) + 4k^2\eta^2\frac{\sin^2 T(\eta)(3-4\sin^2 T(\eta))}{\sin^4 T(a)}\right]\sin^2\theta, \tag{B8}$$

$$P_Q^{II}(\eta,\theta) = \begin{cases} -\displaystyle\sum_{m+n\neq 2} \frac{nQ_{0,m}Q_{0,n}}{4\pi(m+n-2)}\frac{\Lambda^{\frac{m+n}{2}}(\eta)}{\eta^2(1-\eta^2)^{1+(m+n)/4}}\sin^{m+n-2}\theta, & \text{for } m+n\neq 2, \\ -\displaystyle\sum_{m+n=2} \frac{nQ_{0,m}Q_{0,n}}{4\pi}\frac{\Lambda(\eta)}{\eta^2(1-\eta^2)^{\frac{3}{2}}}\log(\sin\theta), & \text{for } m+n=2. \end{cases} \tag{B9}$$

The function D is given by

$$D^{II}(\eta,\theta) = D_0(\eta) + D_A^{II}(\eta,\theta) + D_Q^{II}(\eta,\theta), \tag{B10}$$

where D_A^{II} and D_Q^{II} are

$$D_A^{II}(\eta,\theta) = \frac{A_0^2 a^4}{4\pi GM\eta^3}\Lambda(\eta)\left[d_0(\eta)+d_1(\eta)+d_2(\eta)+d_3(\eta)\right]\sin^2\theta, \tag{B11}$$

$$D_Q^{II}(\eta,\theta) = -\sum_{m,n}\frac{nQ_{0,m}Q_{0,m}}{4\pi GM\eta(1-\eta^2)^{2+\frac{m+n}{4}}}Y(\eta,\theta). \tag{B12}$$

The functions d_0, d_1, d_2, d_3, and Y are given by

$$d_0(\eta) = \frac{3\eta^4-12\eta^2+8}{(1-\eta^2)^3}\Lambda(\eta), \tag{B13}$$

$$d_1(\eta) = \frac{4k\eta(2-3\eta^2)}{(1-\eta^2)^2}\frac{\sin^3 T(\eta)\cos T(\eta)}{\sin^4 T(a)}, \tag{B14}$$

$$d_2(\eta) = \frac{4k^2\eta^2(2+3\eta^2)}{1-\eta^2}\frac{\sin^2 T(\eta)(3-4\sin^2 T(\eta))}{\sin^4 T(a)}, \tag{B15}$$

$$d_3(\eta) = -8k^3\eta^3\frac{\sin T(\eta)\cos T(\eta)(3-8\sin^2 T(\eta))}{\sin^4 T(a)}, \tag{B16}$$

$$Y(\eta,\theta)=\begin{cases}\dfrac{\Lambda^{\frac{m+n-2}{2}}(\eta)}{m+n-2}\left[(2-\eta^2)\Lambda(\eta)+4k\eta(1-\eta^2)\dfrac{\sin^3 T(\eta)\cos T(\eta)}{\sin^4 T(a)}\right]\sin^{m+n-2}\theta, & \text{for } m+n\neq 2,\\ \dfrac{1}{2}\left[\eta^2+2(2-\eta^2)\log(\sin\theta)\right]\Lambda(\eta)+2k\eta(1-\eta^2)(-1+2\log(\sin\theta))\dfrac{\sin^3 T(\eta)\cos T(\eta)}{\sin^4 T(a)}, & \text{for } m+n=2.\end{cases} \tag{B17}$$

The functions P_0 and D_0 are related each other through equation (48).

APPENDIX C: THE VIRIAL THEOREM OF THE SELF-SIMILAR RELATIVISTIC MHD

The virial theorem in non-relativistic MHD was derived by Chandrasekhar & Fermi (1953). Low (1982) applied it to the expanding magnetic loops by evaluating the surface term. Landau & Lifshitz (1975) derived the theorem for a relativistic case in elegant way by integrating the energy momentum tensor. In this appendix, we derive the virial theorem for a relativistic self-similar MHD.

We start from the equations of motion in self-similar stage given by (36). Taking the inner product with $\boldsymbol{r}$ and integrating it within a volume V, we obtain

$$\int dV\left[\frac{\Gamma}{\Gamma-1}\frac{p\gamma^2v^2(\boldsymbol{r}\cdot\boldsymbol{e}_r)}{r}-\boldsymbol{r}\cdot\nabla p+\boldsymbol{r}\cdot(\rho_e\boldsymbol{E}+\boldsymbol{j}\times\boldsymbol{B})-\frac{GM\gamma\rho}{r^2}(\boldsymbol{r}\cdot\boldsymbol{e}_r)\right]=0. \tag{C1}$$

The first term is the thermal inertial term $U_{\rm in}$ and the forth term is the gravitational potential energy W. Integrating the second term by parts, we obtain

$$\int dV\boldsymbol{r}\cdot\nabla p=-3(\Gamma-1)U_{\rm th}+\int p\boldsymbol{r}\cdot d\boldsymbol{\mathcal{A}} \tag{C2}$$

where $\boldsymbol{\mathcal{A}}$ is a closed surface of the volume V. The third term can be rewritten by using the Maxwell equations as follows,

$$\int_V dV\left[\boldsymbol{r}\cdot(\rho_e\boldsymbol{E}+\boldsymbol{j}\times\boldsymbol{B})\right]=-\int dV\frac{\partial}{\partial t}(\boldsymbol{r}\cdot\boldsymbol{S})-\int dV\boldsymbol{r}\cdot(\nabla\cdot\boldsymbol{\sigma}), \tag{C3}$$

where $\boldsymbol{S}$ and $\boldsymbol{\sigma}$ are the Poynting flux and the Maxwell's stress tensor, respectively. Note that the time derivative cannot be exchanged with the integration with volume in the first term since the volume V changes with time.

The second term on the right hand side of equation (C3) has a form

$$-\int dV\boldsymbol{r}\cdot(\nabla\cdot\boldsymbol{\sigma})=U_{\rm E}+U_{\rm M}+\frac{1}{8\pi}\int\left\{2\left[(\boldsymbol{r}\cdot\boldsymbol{E})(\boldsymbol{E}\cdot d\boldsymbol{\mathcal{A}})+(\boldsymbol{r}\cdot\boldsymbol{B})(\boldsymbol{B}\cdot d\boldsymbol{\mathcal{A}})\right]-(\boldsymbol{E}^2+\boldsymbol{B}^2)(\boldsymbol{r}\cdot d\boldsymbol{\mathcal{A}})\right\}, \tag{C4}$$

where $U_{\rm E}$ and $U_{\rm M}$ are the electric and magnetic energies given by equations (75) and (76), respectively. By using these results, we obtain the virial theorem for the relativistic self-similar MHD;

$$3(\Gamma-1)U_{\rm th}+U_{\rm in}+U_{\rm M}+U_{\rm E}+W=\mathcal{H}+\mathcal{S}, \tag{C5}$$

where

$$\mathcal{H}=\int p\boldsymbol{r}\cdot d\boldsymbol{\mathcal{A}}-\frac{1}{8\pi}\int\left\{2\left[(\boldsymbol{r}\cdot\boldsymbol{E})(\boldsymbol{E}\cdot d\boldsymbol{\mathcal{A}})+(\boldsymbol{r}\cdot\boldsymbol{B})(\boldsymbol{B}\cdot d\boldsymbol{\mathcal{A}})\right]-(\boldsymbol{E}^2+\boldsymbol{B}^2)(\boldsymbol{r}\cdot d\boldsymbol{\mathcal{A}})\right\}, \tag{C6}$$

and

$$\mathcal{S}=\int dV\frac{\partial}{\partial t}\left(\boldsymbol{r}\cdot\frac{\boldsymbol{E}\times\boldsymbol{B}}{4\pi}\right). \tag{C7}$$

Here, K is the kinetic energy given by equation (72).

Readers may wonder why the thermal inertial term appears. Actually, the kinetic, thermal, and thermal inertial energies should not be considered separately because they depend on the frame of reference. Even so, we used this definition through the paper to make clear the difference between the non-relativistic and relativistic expansions. We can easily figure out that the total plasma energy can be described as the sum of these energies, as

$$K+U_{\rm th}+U_{\rm in}=\int dV\left[\left(\rho+\frac{\Gamma}{\Gamma-1}p\right)\gamma^2-p\right]. \tag{C8}$$